LAND-ATMOSPHERE INTERACTION AND CLIMATE VARIABILITY

A Dissertation
Presented to
The Academic Faculty

by

Jiangfeng Wei

In Partial Fulfillment
of the Requirements for the Degree
Doctor of Philosophy in the
School of Earth and Atmospheric Sciences

Georgia Institute of Technology
August 2007

LAND-ATMOSPHERE INTERACTION AND CLIMATE VARIABILITY

Approved by:

Dr. Robert E. Dickinson, Advisor
School of Earth and Atmospheric Sciences
Georgia Institute of Technology

Dr. Judith A. Curry
School of Earth and Atmospheric Sciences
Georgia Institute of Technology

Dr. Marc Stieglitz
School of Civil and Environmental Engineering
Georgia Institute of Technology

Dr. Rong Fu
School of Earth and Atmospheric Sciences
Georgia Institute of Technology

Dr. Serge Guillas
School of Mathematics
Georgia Institute of Technology

Date Approved: May 2, 2007

To my family in China and my wife Yun

ACKNOWLEDGEMENTS

I wish to thank Prof. Robert Dickinson for advising my thesis and providing support for my PhD study for the past five years. This dissertation would be impossible without his continuous encouragement and support. I am grateful to the support and help from and discussions with Prof. Ning Zeng (U. Maryland), Prof. Guiling Wang (U. Connet.), Prof. Haishan Chen (Nanjing Inst. Meteor.), and Dr. Jingyong Zhang (SUNY, Albany). I also like to thank my current and past group members Drs. M. Shaikh, Wanru Wu, Qing Liu, Liming Zhou, Yuhong Tian, Yan Huang, Huiling Gao, Mi Zhou, Yan Zhang, Yanping He, and Willis Shem for their kindness and numerous help.

I wish to thank my family in China for their nourishment and support for so many years, and my wife for encouragement during hard times of this study.

ECMWF ERA-40 data used in this study have been obtained from the ECMWF data server. R-2 and NARR data is provided by the NOAA/OAR/ESRL PSD, Boulder, Colorado, USA, from their Web site at http://www.cdc.noaa.gov/. GSWP-2 data is from its website at http://www.iges.org/gswp/. Cross-wavelet and wavelet coherence software were provided by A. Grinsted.

TABLE OF CONTENTS

LIST OF TABLES

LIST OF FIGURES

LIST OF ABBREVIATIONS

BATS	Biosphere Atmosphere Transfer Scheme
ET	evapotranspiration
GCM	general circulation model
GLACE	Global Land-Atmosphere Coupling Experiment
GSWP	Global Soil Wetness Project
LAI	leaf area index
NARR	North American Regional Reanalysis
NDVI	normalized difference vegetation index
PAR	photosynthetically active radiation
PE	precipitation efficiency
SiB	Simple Biosphere Model
S-P	soil moisture-precipitation

SUMMARY

Land-atmosphere interaction includes complex feedbacks among radiative, hydrological, and ecological processes, and the understanding of it is hindered by many factors such as the heterogeneity of land surface properties, the chaotic nature of the atmosphere, and the lack of observational data. In this study, several different methods are used to investigate the land-atmosphere interaction processes and their relationship with climate variability.

Firstly, a simple one-dimensional model is developed to simulate the dominant soil-vegetation-atmosphere interaction processes in the warm climate. Although the physical processes are described coarsely, the model can be more easily used to find some relationships which may be drown out or distorted by noise. The influence of land on climate variability mainly lies in it memory, which is greatly related with the atmospheric forcing, so this model is used to investigate the influence of different forcing strengths on land-atmosphere interaction and its difference at different land covers. The findings from the simple model can provide guidance for other studies.

The second part of the study compares a lagged soil moisture-precipitation (S-P) correlation (soil moisture in current day and precipitation in future 30 days) in three atmospheric reanalysis products (ERA-40, NCEP/DOE reanalysis-2, and North American Regional Reanalysis (NARR)), Global Soil Wetness Project Phase 2 (GSWP-2) data, and NCAR CAM3 simulations. Different datasets and model simulations come to a similar negative-dominant S-P correlation pattern with wet areas having more significantly negative correlations than the dry areas. This is different from the

traditional view that the soil moisture should have positive influence on future precipitation. Further analysis shows that this correlation pattern is not caused by the soil moisture feedback but due to the combined effect of the precipitation oscillation and the memory of soil moisture. Theoretical analysis confirms the above results and finds that the precipitation time series with the strongest oscillation at 32-60 day period is most likely to induce a significantly negative S-P correlation, and regions with longer soil water retention time are more likely to have a significantly negative S-P correlation. This study illustrates that a lagged correlation does not always indicate a causal relation.

CHAPTER 1

INTRODUCTION

1.1 Basics of land-atmosphere interaction

1.1.1 Energy and water balance

Land surface is an important component of the climate system. It controls the partitioning of available energy at the surface between sensible and latent heat, and controls the partitioning of available water between evaporation and runoff. Land-atmosphere interaction is essentially the exchanges of water and energy between land surface and atmosphere.

The net radiation at surface

$$R_n = S\downarrow(1-\alpha) + L\downarrow - L\uparrow, \tag{1.1}$$

where $S\downarrow$ is the downward solar radiation, α is surface albedo, $L\downarrow$ and $L\uparrow$ are the downward and upward longwave radiation at the surface. α is related with soil type and wetness, vegetation texture and physiological condition, snow cover, etc. $L\downarrow$ and $L\uparrow$ is related with temperature and emissivity of land and atmosphere. R_n must be balanced by the surface sensible heat flux (*SH*), latent heat flux (*LH*), and soil heat flux (*G*):

$$R_n = SH + LH + G. \tag{1.2}$$

SH and *LH* are sensitive to the nature of land surface and have direct influence on convection and precipitation.

The partitioning of precipitation *P* at surface can be expressed as a water balance equation

$$P = E - R - \Delta S\,, \tag{1.3}$$

where E is evapotranspiration (ET), R is runoff, and ΔS is soil moisture change. The surface water balance is also greatly affected by the surface characteristics. For example, the vegetation characteristics and distribution affect the interception, transpiration, and soil evaporation. The water balance (Eq. 1.3) and energy balance (Eq. 1.2) are connected by LH and E as

$$LH = \lambda E\,, \tag{1.4}$$

where λ is latent heat of vaporization.

1.1.2 Soil water and vegetation dynamics

Soil and vegetation are two main components of land surface. In this section, I will use some simple equations to describe the processes of soil water and vegetation variations. Their dynamics can be easily understood by studying these equations.

The water balance equation (1.3) can be in a derivative form as

$$\frac{dS}{dt} = P - E - R\,. \tag{1.5}$$

E can be simply related with soil water S as (a more complex form is given in chapter 2.2.1)

$$E = E_p(\frac{S}{S_{fc}})\,, \tag{1.6}$$

where E_p is potential evaporation, S_{fc} is field capacity of soil. Eq. (1.6) shows how soil wetness controls the evaporation. Substitute (1.6) in to (1.5), we can get

$$\frac{dS}{dt} = -\alpha S + F\,, \tag{1.7}$$

where $\alpha = E_p / S_{fc}$, and $F = P - R$. F can be regarded as a forcing to soil water S.

The vegetation dynamics can be simply expressed following Zeng et al. (1999)

$$\frac{dV}{dt} = a\beta(S)(1-e^{-kV}) - V/\tau, \tag{1.8}$$

where V is leaf area index or vegetation carbon, a is a carbon assimilation coefficient, $\beta(S)$ is soil water stress for vegetation growth, k is a parameter related with radiation, τ is the time scale of vegetation growth. More detailed explanation can be found in chapter 2.2.3. Eq. (1.8) can also be simplified as

$$\frac{dV}{dt} = -\alpha V + F, \tag{1.9}$$

where F is the first term on the rhs of Eq. (1.8), and can be regarded as a (precipitation and radiation) forcing to vegetation. $\alpha = 1/\tau$.

It is easy to find that Eqs. (1.7) and (1.9) have a similar form: the time derivative of the variable equals a damping term plus a forcing. This kind of equation is called the damped oscillator in physics (the acceleration is 0). A property of this kind of equation is that if F is a white noise forcing, S or V will be a red noise (Delire et al. 2004). Therefore, these equations describe how the soil water and vegetation processes are slower than the atmospheric processes.

The phase and amplitude relations between the forcing F and the response variable S or V can also be studied. Let's take Eq. (1.7) as an example. Assume F is a periodic forcing $F = F_0 e^{i\omega t}$. Substitute it into (1.7) and solve S. We can get

$$S = \frac{F_0(\alpha - i\omega)e^{i\omega t}}{\alpha^2 + \omega^2}. \tag{1.10}$$

The amplitude of S relative to F is

$$\left|\frac{S}{F_0}\right|^2 = \frac{1}{\alpha^2 + \omega^2}, \tag{1.11}$$

and the phase lag of S relative to F is

$$\phi = \arctan(\frac{\omega}{\alpha}). \tag{1.12}$$

Their relations with forcing frequency ω are plotted in Figure 1.1. It can be seen that the relative amplitude decreases with forcing frequency, while the phase lag increases with forcing frequency. This can be easily understood: low-frequency forcing can make soil and vegetation have more time to respond, which leads to larger variance and smaller time lag; if the forcing frequency is high, the soil water and vegetation have little time to respond to the forcing because of their relatively long adjustment time.

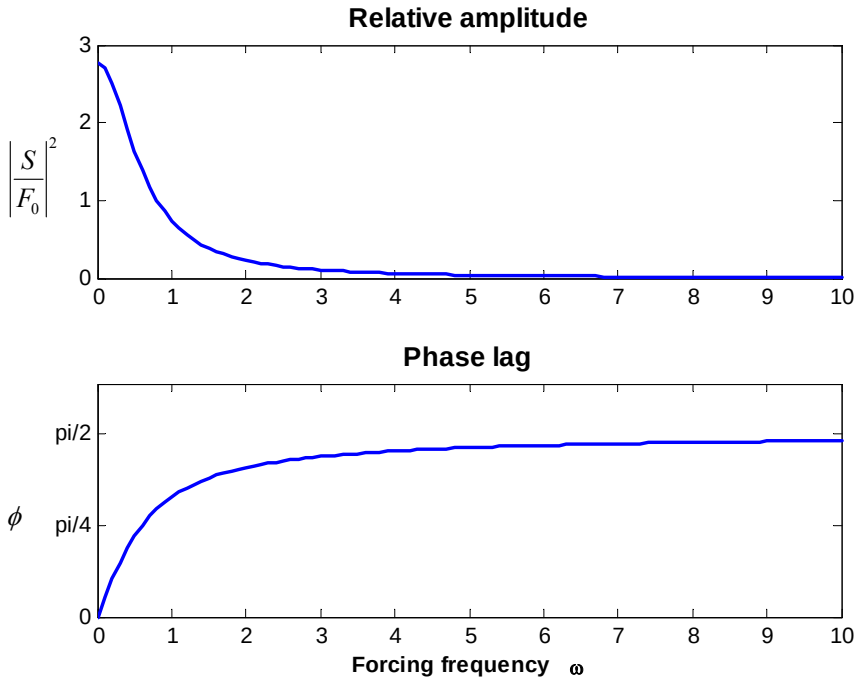

Figure 1.1 Variations of the relative amplitude (Eq. 1.11) and phase lag (Eq. 1.12) with forcing frequency ω. α is given as 0.6.

It can be noted that the vegetation dynamics (Eq. 1.8) is influenced by the soil water dynamics (Eq. 1.5) through the soil water *S*. In fact, vegetation also influences soil water through canopy shading, water absorbing by root, etc. Thus it is interesting to study their interactions and how the atmosphere interacts with them. This is the purpose of Chapter 2.

1.2 Evolution of land surface models

Observations of land surface variables are very limited. Modeling can provide more comprehensive data and the capability to analyze causality, so it is still a major method in current research. Sellers et al. (1997) and Pitman (2003) have given very good reviews of the evolution of land surface schemes in climate models. I will give a brief introduction based on their papers. The land surface models talked about here are components of climate models, which are designed to simulate large spatial scale and long temporal scale processes.

The simple land model of Manabe (1969) is representative of the first-generation land models. This model has one soil layer of constant depth and water-holding capacity globally. The evaporation is limited by soil moisture if it is below a certain threshold, and if the soil moisture exceeds a limit further precipitation will generate runoff. This parameterization is commonly called "bucket model" because it describes the land as a bucket to hold water. Although it is simple, this model cannot be distinguished from more complex schemes for the simulated soil moisture and climate at long timescales, because the ET is calculated properly (Henderson-Sellers et al. 1995; Desborough 1999). The weakness of the first-generation models includes uniform water-holding capacity, no

explicit canopy resistance in ET calculation, and the use of the same aerodynamic resistance for heat, water, and momentum. The first-generation models did not provide a suitable framework to enable modeling of CO2 exchange, or to enable experiments to be performed to explore the impacts of land cover change.

Deardorff (1978) introduced a method for simulating soil temperature and moisture in two layers and vegetation as a single bulk layer. This represented a revolution in land surface modeling, since the processes were treated explicitly and this provided a framework for people to contribute. The two key contributors were R. E. Dickinson and P. J. Sellers, who developed their respective land schemes, the Biosphere Atmosphere Transfer Scheme (BATS; Dickinson et al. 1986, 1993) and Simple Biosphere Model (SiB; Sellers et al. 1986, 1996), based on the philosophy of Deardorff (1978). These two models represented the second-generation land model. There are a very large number of second-generation models that are innovative in the way some components have been developed or tested, but all are fundamentally built from the leadership of Deardorff, Dickinson, and Sellers. The second-generation models differentiate between soil and vegetation at the surface, so albedo may vary spatially across a grid square and vary depending on the wavelength of the incoming solar radiation. Canopies are rough and generate turbulence, which enhances the exchange of sensible and latent heat fluxes. Plants regulate water use to maximize their ability to fix carbon via photosynthesis. The second-generation models provide the basis for almost all recent estimates of the impact of increasing CO2 on climate (Houghton et al. 2001).

The major advance of second-generation models is that they take into account plant and environmental conditions to model canopy conductance empirically. It was

recognized in the late 1980s that the addition of an explicit canopy conductance provide a means not only to improve the simulation of ET pathway, but also to address the issue of carbon uptake by plants. The addition of carbon into land models represented a major revolution in the modeling capability and indicated the beginning of the third generation land models. This revolution needed the support of the plant physiology community. They had established that the leaf assimilation of carbon was limited by the efficiency of the photosynthetic enzyme system (Rubisco-limitation), the amount of photosynthetically active radiation (PAR) captured by the leaf chlorophyll, and the capacity of the leaf to utilize the products of photosynthesis. Partitioning of accumulated carbon during growth is not a traditional area of expertise in land surface modeling (which is limited to the top two boxes of Figure 1.2), but it is within the ecological community. Dickinson et al. (1998) allocate carbon to leaves, convert it to carbon assimilation per unit leaf area and thus allow leaves to grow. They also allow for root and wood allocation and use a simple soil carbon model based on Parton et al. (1987). Thus, an land model that has been able to respond to changes in climate through influencing energy and water exchange can now respond in two further ways to a climate change: physiologically as increasing CO2 influences the canopy conductance and structurally by growing different leaves or taller trees (third box, Figure 1.2). Evidence already exists to show that representing these two feedbacks is important (Henderson-Sellers et al., 1995; Pollard and Thompson, 1995; Betts et al., 1997; Levis et al., 2000; Bergengren et al., 2001). Overall, the addition of these processes represents a fundamental advance in land models towards a realistic representation of significant feedbacks that are missing in climate simulations of increasing CO2: the response of the biosphere. Thus, third-generation schemes are

identifiable by the method used to model carbon. These models tend to represent other processes (soil temperature, soil hydrology, runoff, etc.) similarly to those included in second-generation models.

As land-surface modelers were building the land model, they have observed the parallel development of a suite of ecological models by a different community. These ecological models tended to focus on carbon and other biogeochemical cycles (bottom two boxes of Figure 1.2), use plant functional relationships to categorize the vegetation (Bonan et al., 2002). These ecological models tended to focus on how the terrestrial biosphere responded to the atmosphere (on time scales of months to years) rather than how the land surface partitioned energy and water as a boundary condition for the atmosphere. The Foley et al. (1996) model is an example of a group known as dynamic global vegetation model (DGVM). Other intercomparisons and discussions of these terrestrial ecosystem models are provided by McGuire et al. (2001) and Cramer et al. (2001). The merging of the ecological approaches with land models (i.e. the full complexity of Figure 1.2) is extremely challenging, but it opens up major opportunities to link the physical and biophysical sciences and provides tools to begin to address key questions regarding the future of global-scale biogeochemical cycles.

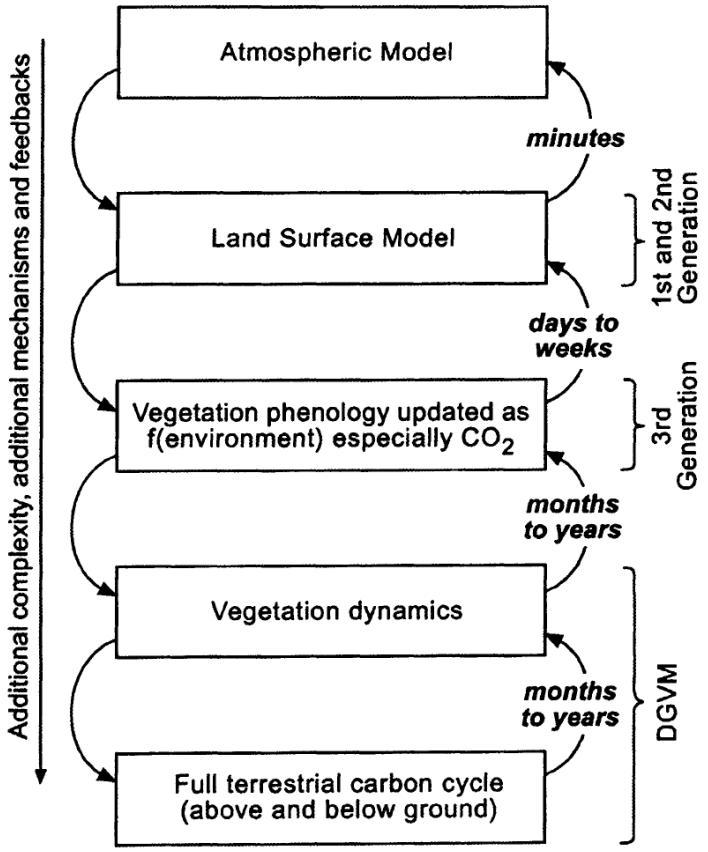

Figure 1.2 Schematic of the increasing levels of detail being added into land surface modeling. The second box represents first- and second-generation land surface models. The addition of vegetation phenology (via semi-mechanistic models of leaf photosynthesis and respiration) defines third-generation models. The allocation of the net carbon balance, and other additions to reflect the full terrestrial carbon cycle translates a 'land surface scheme' into a DGVM. In each case, the requirements are additive, so that a fully coupled DGVM requires the traditional (usually second-generation) land surface model. From Pitman 2003.

1.3 Impact of land on weather and climate

The impact of land cover change on climate has been a concern since the 1970s (e.g., Charney, 1975; Charney et al., 1977). At that time, the studies are limited to albedo changes because the second-generation land models with explicit vegetation representations were not yet available. The development of second-generation land models and their coupling with atmospheric models enabled the community to address the problem of land cover change on climate. Many modeling studies have been done on the climate changes caused by land cover changes in the African Sahel (e.g., Xue and Shukla, 1993; Zheng and Eltahir, 1997; Clark et al., 2001; Taylor et al., 2002), the Amazon [e.g., Dickinson and Henderson-Sellers, 1988; Lean and Warrilow, 1989; Dickinson and Kennedy, 1992), and some other regions (e.g., Xue, 1996; Fu, 2003). Almost all the studies have demonstrated that large-scale deforestation may lead to decreased precipitation and increased temperature, although the prescribed deforestation areas are largely exaggerated in order to get strong enough response to fight the uncertainties of the models.

The increase of computer power and the completeness of prediction models enable the investigation on predictability of short-term climate. A famous example is the Dynamical Seasonal Prediction (DSP) Project (Shukla et al. 2000). The basic idea of the project is to test the feasibility of extending the technology of routine numerical weather prediction beyond the inherent limit of deterministic predictability of weather to predict climate using global atmospheric models. As atmospheric chaos severely limits the predictability of precipitation on seasonal time scales, the hope for an accurate seasonal forecast lies with simulating the atmospheric response to the slowly varying states of the

ocean and land surface, which can be predicted weeks to months in advance. Dirmeyer (2003) showed that while SST appears to be the dominant factor in providing skill to boreal winter forecast over land, in other seasons the land surface state affects skill. The land surface states include variables such as soil moisture and temperature, vegetation states, snow cover, and surface water stores. At time scales less than a year and for majority of the land, soil moisture is perhaps the most important (Wei et al. 2006). The degree of impact of land surface on climate varies from model to model, but numerous studies in recent years have shown significant positive impact on the skill of seasonal hindcasts by application of realistic soil wetness initial conditions (e.g., Fennessy and Shukla 1999; Koster and Suarez 2003; Kanamitsu et al. 2003), boundary conditions (e.g., Dirmeyer 2000; Douville 2003; Dirmeyer and Zhao 2004), and even snow cover (e.g., Yang et al. 2001; Schlosser and Mocko 2003).

In order to further investigate where on Earth the land has strongest influence on precipitation and how strong the influence is, the Global Land-Atmosphere Coupling Experiment (GLACE; Koster et al. 2004, 2006; Guo et al. 2006) is initiated. A dozen climate-modeling groups have performed the same highly controlled numerical experiments. The derived coupling strengths vary widely. However, enough similarity is found in the spatial patterns generated by the models to pinpoint the "hot spots" of land-atmosphere coupling. The hot spots are mainly the transitional zones between wet and dry climate, for example, for boreal summer, such hotspots for precipitation and temperature are found over African Sahel, central North America, and Indian; a hot spot for temperature is also found over large regions of eastern China.

A problem accompany that of the influence of land on climate predictability is the influence of land on climate variability. The extreme climate (e.g., drought and flood) associated with climate variability may be more important for us than the mean climate. The pioneer study of Delworth and Manabe (1988, 1989) first illustrated with model experiments that the interaction of soil moisture and atmosphere can lengthen the timescale of surface humility and temperature and increase the total variability of atmosphere. Koster and Suarez (1995) and Koster et al. (2000) showed that land surface processes can contribute significantly to the variance of precipitation over continent. Dickinson (2000) analyzed this problem theoretically. Voldoire and Royer (2004) showed that land cover change can impact not only the mean climate but also the climate variability. Recently, Seneviratne et al. (2006) discovered that soil moisture feedback plays a crucial role in the Europe summer heat wave (temperature variability) caused by global warming. In addition to soil moisture feedback, vegetation interaction also plays an important role, but on longer timescales. The development of dynamic vegetation models enables the study of vegetation-climate interaction. Using coupled vegetation-climate models, Zeng et al. (1999) and Wang and Eltahir (2000) found that vegetation-climate interaction can enhance the decadal precipitation variability in the tropics, which is an important factor that may has contributed to the Sahel drought.

With the development of models, satellite remote sensing, local observations, and analytical techniques, the land-atmosphere interaction study has been advanced in many other different directions. By analyzing the normalized difference vegetation index (NDVI) from satellite data and its relation with climate variables, Myneni et al. (1997) and Zhou et al. (2001) found that the vegetation growth in the Northern latitudes is

promoted by global warming. Roger Pielke and his colleagues used mesoscale simulations and observations to study the regional land use and land cover change on local weather (e.g., Pielke et al. 2007). Kalnay and Cai (2003) calculated the temperature difference between NCAR/NCEP reanalysis and station observations and used it to estimate the influence of urbanization on local surface temperature.

1.4 Objectives and outline of this study

The main content of this thesis includes two parts (chapters), which are two different studies of land-atmosphere interaction and climate variability.

In chapter 2, a simple model of soil-vegetation-atmosphere interaction is developed to study the land-atmosphere interaction and climate variability in a warm climate (where soil-vegetation-atmosphere interaction is strong). Several questions are addressed with the model:

1) When does the vegetation-climate system have multiple equilibrium states?
2) What are the roles of soil moisture and vegetation feedback in the climate variability at different land covers, and how they change with external forcing?
3) What are the roles of vegetation and external forcing in the soil moisture-precipitation relation?

Chapter 3 compares a lagged soil moisture-precipitation (S-P) correlation in three atmospheric reanalysis products (ERA-40, NCEP/DOE reanalysis-2, and North American Regional Reanalysis), GSWP-2 data, and NCAR CAM3 simulations. Different datasets and model simulations come to a similar negative-dominant S-P correlation pattern with wet areas having more significantly negative correlations than the dry areas. Model

simulations and theoretical analyses are used to investigate the causes of this relation. Although it is finally found that this lagged relation does not indicate a causal relationship between soil moisture and precipitation, this study increases our understanding of S-P interaction.

The major conclusions are given in Chapter 4.

CHAPTER 2

LAND-ATMOSPHERE INTERACTION AND CLIMATE VARIABILITY IN A SIMPLE MODEL

2.1 Background

Land-atmosphere interaction includes complex feedbacks among soil, vegetation, and atmosphere (e.g., Rodriguez-Iturbe et al., 1999a), and the understanding of it is hindered by the heterogeneity of land surface properties and the chaotic nature of the atmosphere. All kinds of efforts (e.g., remote sensing, field experiments) are made to study these processes. Currently, modeling is still a primary approach due to limited observations, especially for long-timescale and large-space-scale processes.

Land surface models have advanced from a bucket-type parameterization in the 1960s to the current soil-vegetation-atmosphere interactive schemes with carbon cycle (see chapter 1.2). However, intercomparison shows that different land models, even with the same atmospheric forcing, still give significantly different surface fluxes and soil wetness (Henderson-Sellers et al., 1995). These differences come from the different parameterizations of individual processes and the amplification of the differences by the nonlinearity of the models. Complex models include detailed description of various processes, but the useful signals are often drowned out by all kinds of noise. These complex models are not always suitable for mechanistic study, so various simple models have been developed and are proven to be efficient for some purposes (e.g., Rodriguez-Iturbe et al., 1991; Zeng, 1998; Liu and Avissar, 1999; Zeng et al., 2004). As noise in real

climate system or GCMs (general circulation models) may distort some of the relationships or even make them indiscernible, simple models which properly describe the important processes can be more easily used to find such relationships. Current climate models are not only complex but also computationally expensive, and most simulations are performed without a hypothesis as to the expected results, so simulations often have to be done several times to select the best experimental design. Such repetition can be very time and energy consuming for studying longer periods. It is thus preferable to obtain some qualitative results to guide the long-term integration of GCMs.

Soil and vegetation are two main components of land surface, and they are the primary sites for the exchange of water, energy, and momentum between land and atmosphere. As soil moisture and vegetation change have memories considerably longer than most of the atmospheric processes, coupling them to the atmosphere can contribute to the skill of climate simulation from seasonal (Delworth and Manabe, 1989; Koster and Suarez, 1995; Koster et al., 2000, 2004; Xue et al., 2004; Levis and Bonan, 2004) to decadal timescales (Zeng et al., 1999; Wang and Eltahir, 2000a; Wang et al., 2004; Delire et al., 2004; Brovkin et al., 2003). Because of the limitations of computational resources and models, simulations with coupled GCM-DGVMs (dynamic global vegetation model) are still not very common. Most current studies of land-atmosphere interaction focus on the feedback between soil moisture and precipitation and the vegetation is fixed at seasonal climatologies. But in reality the vegetation will change with climate and has some memory, so it will not immediately recover after a drought or a long dry season. A main purpose of this study is to reveal how the interactive vegetation influences land-

atmosphere interaction and the simulated climate variability, especially the coupling of soil moisture and precipitation.

We assumed that the region studied is warm enough throughout the year, so that temperature is not a stress for ET and vegetation growth, and most precipitation is convective (e.g. tropical land). Based on this assumption, a simple model of warm climate land-atmosphere interaction is developed. It includes land surface processes important for long-term land-atmosphere interaction, and an empirical relation between precipitation and other variables. The model is then used to study the role of interactive soil moisture and vegetation in climate variability and predictability. Monthly to seasonal timescale processes are the focus of this paper.

2.2 Model Description

A one-dimensional model is developed to simulate the major physical and biophysical processes in warm climate land-atmosphere interaction. It includes bulk soil hydrology, dynamic vegetation, and land-atmosphere interaction processes--ET and precipitation. The model simulates the land surface fluxes at large spatial and long temporal scales by statistically taking into account smaller and faster scale variations, so it is suitable for monthly to decadal scale study. It is not intended to give a precise description of all kind of processes, but to focus on their interaction and hence study the role of these processes in climate variability.

2.2.1 Evapotranspiration

It is assumed that the vegetated area and bare ground are evenly distributed and they have the same soil moisture after spatial interaction. ET is described here using a set of simplified formulas. Evaporation from the bare ground is calculated as

$$E_b = E_p \eta(S), \tag{2.1}$$

where E_p is potential ET, η is water stress for evaporation over ground ($0 \leq \eta \leq 1$) (Dingman, 2002), and S ($0 \leq S \leq 1$) is soil wetness (ratio of volumetric soil water content to soil porosity). We assumed that under the land surface change, the change in ET due to soil wetness and vegetation changes dominates over other effects such as wind and humidity changes, so E_p is given as a constant. η is a function of soil moisture and soil properties. If soil properties do not change, it is only a function of soil moisture

$$\eta(S) = [(S - S_{wp})/(S_{fc} - S_{wp})]^c, \tag{2.2}$$

where S_{wp} is soil wilting point, and S_{fc} is field capacity. When $S < S_{wp}$, $\eta = 0$. The exponent c accounts for the possible nonlinear dependence of evaporation on water deficit.

Vegetation shading is accounted for by taking the soil evaporation under the vegetation as

$$E_v = E_p \eta(S) e^{-k_b L} \tag{2.3}$$

where L is leaf area index (LAI), and k_b is the canopy extinction coefficient that controls what fraction of the soil surface beneath a canopy is directly exposed to the atmosphere above the canopy (Campbell and Norman, 1998). As the interception and transpiration may compensate each other with almost no change in the total (Wang and Eltahir, 2000b), and their effects on soil moisture are also the same, transpiration and interception losses are lumped as

$$TI = E_p \beta(S)(1 - e^{-k_b L}), \tag{2.4}$$

where $\beta(S)$ is vegetation water stress and is defined as

$$\beta(S) = [(S - S_{wp}(1 - \frac{L_w}{L_x}))/(S_{fc} - S_{wp}(1 - \frac{L_w}{L_x}))]^q . \tag{2.5}$$

This expression is similar to evaporation water stress in Eq. (2.2) but accounts for water uptake by roots from deep layers by decreasing total S_{wp} with increasing rooting depth, and the rooting depth is assumed to be proportional to L_w (see chapter 2.2.3 for L_w and L_x). Exponent q accounts for the nonlinear dependence of vegetation water stress on soil saturation in the bulk model (Rodriguez-Iturbe et al., 1999b).

The fraction of vegetation coverage is approximated as

$$f = L / L_x, \tag{2.6}$$

where L_x is the maximum LAI given as 6. The total ET from this area, including vegetated and bare land, is

$$ET = f(E_v + TI) + (1 - f)E_b . \tag{2.7}$$

2.2.2 Soil hydrology

The water budget equation for a single soil layer is

$$D\phi \frac{\partial S}{\partial t} = P - ET - R , \tag{2.8}$$

where D is the depth of hydrologically active soil, ϕ is soil porosity, and P is precipitation. Runoff R includes surface runoff R_s and subsoil gravitational drainage R_d, and is parameterized simply as (e.g., Dickinson et al., 1993)

$$R_s = (P - ET)S^4 , \tag{2.9}$$

$$R_d = K_s S^{2B+3}, \tag{2.10}$$

where K_s is saturated hydraulic conductivity, and B is the Clapp-Hornberger exponent (Clapp and Hornberger, 1978).

2.2.3 Vegetation Dynamics

The simple dynamic vegetation model is based on the simple LAI model of Zeng et al. (1999), but adds a seasonal time-dependence to model the seasonal variation of vegetation (leaf phenology). This model considers the dependence of photosynthesis on soil moisture by retaining the major biophysical aspects of some complex dynamic vegetation models (e.g., Foley et al., 1996; Cramer et al., 2001), but sidesteps the carbon cycle completely. It predicts LAI L once a day as

$$\frac{\partial L}{\partial t} = a\beta(S)(1 - e^{-k_p L}) - \frac{L}{\tau_l}, \tag{2.11}$$

and predicts potential maximum LAI L_w annually as

$$\frac{\partial L_w}{\partial t} = b\beta(S)(1 - e^{-k_p L_w}) - \frac{L_w}{\tau_w}. \tag{2.12}$$

L, $L_w > 0$. The first terms on the rhs of Eqs. (2.11) and (2.12) represent photosynthesis while the second terms represent vegetation losses. Their parameters are: k_p, the extinction coefficient of photosynthetically active radiation, τ_l, the leaf growth (phenology) timescale, τ_w, the timescale of vegetation type transition (succession), and L_w, the maximum leaf area that currently can be supported. Both τ_l and τ_w depend on climate, vegetation and soil properties. L_w is associated with vegetation types, and trees

have larger L_w than grasses because they can support more leaves. For a certain area, L can never exceed L_w. L_w is not related to current LAI and is only related to climate condition and vegetation types. The coefficients *a, b* are chosen such that under optimal climate conditions (β=1) vegetation would grow to its maximum LAI ($L = L_w$, $L_w = L_x$), so

$$a = \frac{L_w}{\tau_l (1 - e^{-k_p L_w})}, \tag{2.13}$$

$$b = \frac{L_x}{\tau_w (1 - e^{-k_p L_x})}. \tag{2.14}$$

Although the vegetation model only describes the natural growth of vegetation, the influence of human activities can be added by prescribing some variables. For example, a sudden deforestation can be included by taking $L = L_w$ =0.01 (this is the prescribed minimum LAI to make vegetation able to start again in the model), and L_w and L can be given values to represent planting. The initial value of L_w depends on the vegetation type planted, and saplings should has larger L_w than seeds.

2.2.4 Precipitation

Precipitation has much uncertainty due to its large temporal and spatial variabilities. In order to decrease these uncertainties, we assumed that the spatial scale we are modeling is regional to continental scale. The precipitable water comes from local ET and horizontal transport, so the precipitation is calculated as

$$P = \text{maximum of}(ET \cdot PE / \rho + \sigma \cdot F(t), 0), \tag{2.15}$$

where PE is precipitation efficiency (PE), ρ is water recycling ratio, F is added external forcing, and σ is its forcing strength. PE is the fraction of input moisture flux that falls as precipitation, and it is associated with both local and large scale factors (Eltahir and Bras, 1996). We express it as

$$PE = PE_{\min} + \alpha[f(1 - e^{-mL}) + (1 - f)S], \tag{2.16}$$

where $PE_{\min}$ is the minimum PE when the land is very dry and has no vegetation, α is the strength of vegetation and soil wetness to trigger and sustain precipitation through the influence of albedo and roughness length (Lofgren, 1995; Eltahir, 1996, 1998), and m is an empirical coefficient. This expression qualitatively considers local impact of vegetation and soil moisture on rainfall.

The water recycling ratio ρ is defined as the ratio of moisture from local ET versus the total of local ET and horizontal transport (Trenberth, 1999). It is influenced by both local and surrounding thermal changes and has a seasonal cycle (Brubaker et al., 1993). It is assumed sinusoidal as

$$\rho = \overline{\rho} + \sigma_{\rho} \sin(2\pi t / T). \tag{2.17}$$

Although other model variables, such as potential ET, temperature stress, and PE, could also have a seasonal cycle like ρ, such are not considered here to maintain simplicity. The constant recycling ratio assumes a linear relationship between ET and horizontal moisture transport. Such is expected in a deep convective region where a small perturbation to local energy balance will cause a large scale atmospheric circulation change such that moisture convergence feedback is quasi-linearly proportional to change in local moisture static energy which includes ET (Zeng and Neelin, 1999). Most warm climate rainfall is deep convective.

The last term of Eq. (2.15) is a random time series to describe the uncertainty of precipitation due to the nonlocal variability, such as from SST variation and ENSO, and the internal variability from atmospheric dynamics. Hereafter, these two variabilities are together referred to as the "external forcing" because they are not from the local land-atmosphere interaction processes described here. F is given as a white noise added onto a red noise to represent different processes and forcings in the atmosphere (F has a mean of 0 and a standard deviation of 1.57 here). In fact, the last term lumps the disturbances of ET, PE and ρ. Although such external forcing could influence almost every part of the land-atmosphere interaction, it is only added to precipitation to keep the simulation simple and aid the physical interpretation of the results.

2.2.5 Model Implementation

The sequence of model calculations is shown in Figure 2.1. Initial soil moistures and vegetation are needed to start the integration. A forward difference scheme is used to integrate the differential equations. Unless otherwise mentioned, the parameter values used in the model are shown in Table 2.1. They are some characteristic values for the tropics and not for a specific area. The time step for the integrations is 1 day, and Eq. (2.12) is integrated once a year. For simplicity, each month is 30 days and each year is 360 days. Considering the coarse parameterization of the model, only monthly mean values of the outputs are used for analysis.

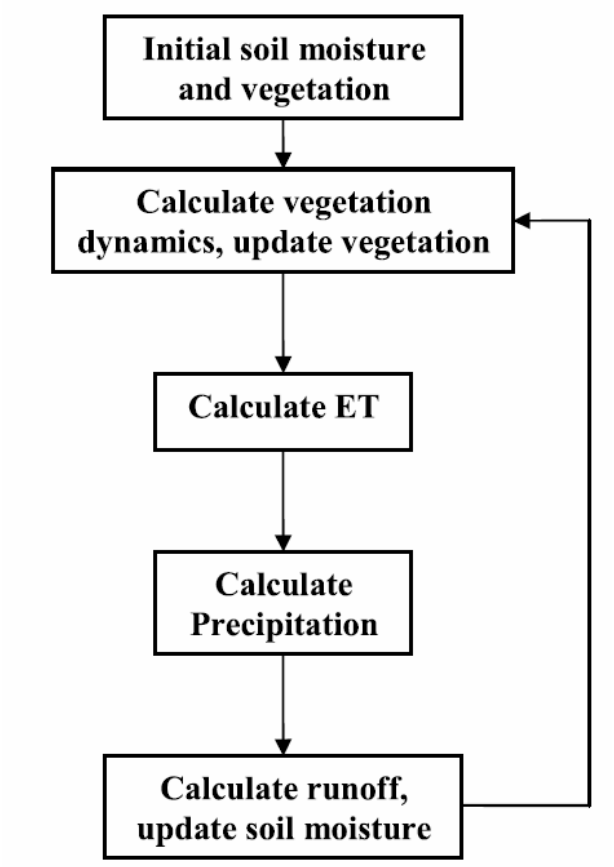

Figure 2.1 Schematic of the model integration cycle.

Table 2.1 Parameter values used in the model

Parameter	Value	Unit	*Source*
E_p	5	mm/day	[*Mintz and Walker*, 1993]
T	360	days	
S_{wp}	0.3		[*Dickinson et al*., 1993]
S_{fc}	0.74		[*Dingman*, 2002]
c	2		[*Lowry*, 1959]
k_b	0.82		[*Campbell and Norman*, 1998]
$D\phi$	1000	mm	[*Entekhabi et al*., 1992]
K_s	1000	mm/day	[*Dickinson et al*., 1993]
B	4		[*Dickinson et al*., 1993]
k_p	0.75		[*Zeng et al*., 1999]
τ_l	10	days	
τ_w	4	years	
q	0.25		[*Rodriguez-Iturbe et al*., 1999b]
$PE_{\min}$	0.2		
α	0.4		
m	0.5		
$\overline{\rho}$	0.3		[*Brubaker et al*., 1993]
σ_ρ	0.1		[*Brubaker et al*., 1993]

2.3 Model Performance and Behavior

2.3.1 Basic performance

The model-simulated mean annual cycle of soil wetness, precipitation, LAI, and ET are shown in Figure 2.2. LAI lags precipitation and soil wetness, which is consistent with observations (Zhang et al., 2005), and the exact time of lag depends on vegetation types (L_w) and leaf phenology (τ_l). Figure 2.3 shows the ET over its potential value as a function of soil saturation for fully vegetated and bare land. Their relationships are nonlinear. Vegetated land has larger ET for the same soil wetness because vegetation can take up water from deep layers, hence making the deep soil drier (Scanlon et al., 2005). If soil wetness is larger than or equal to field capacity, ET is equal to its potential value. The results are consistent with those in Lowry (1959) (also referred to in Rodriguez-Iturbe et al. (1991)). They demonstrate the model's ability to capture the basic features of land surface control on ET.

2.3.2 Multiple equilibrium states

Many studies have demonstrated that a water-constrained biosphere-atmosphere system can have multiple equilibrium states at a certain parameter regime (Zeng and Neelin, 2000; Wang, 2004; Zeng et al., 2004; Liu et al., 2005; D'Odorico et al., 2005), and our model also shows such a feature. Several 50-year runs are performed with different initial L_w values of 2, 3, 4, and 5 to represent different initial vegetation types. All initial LAIs are given as 1 because we found that the initial LAI is not important for long-term variability. Without outside forcing, small initial L_ws tend to lead to a dry

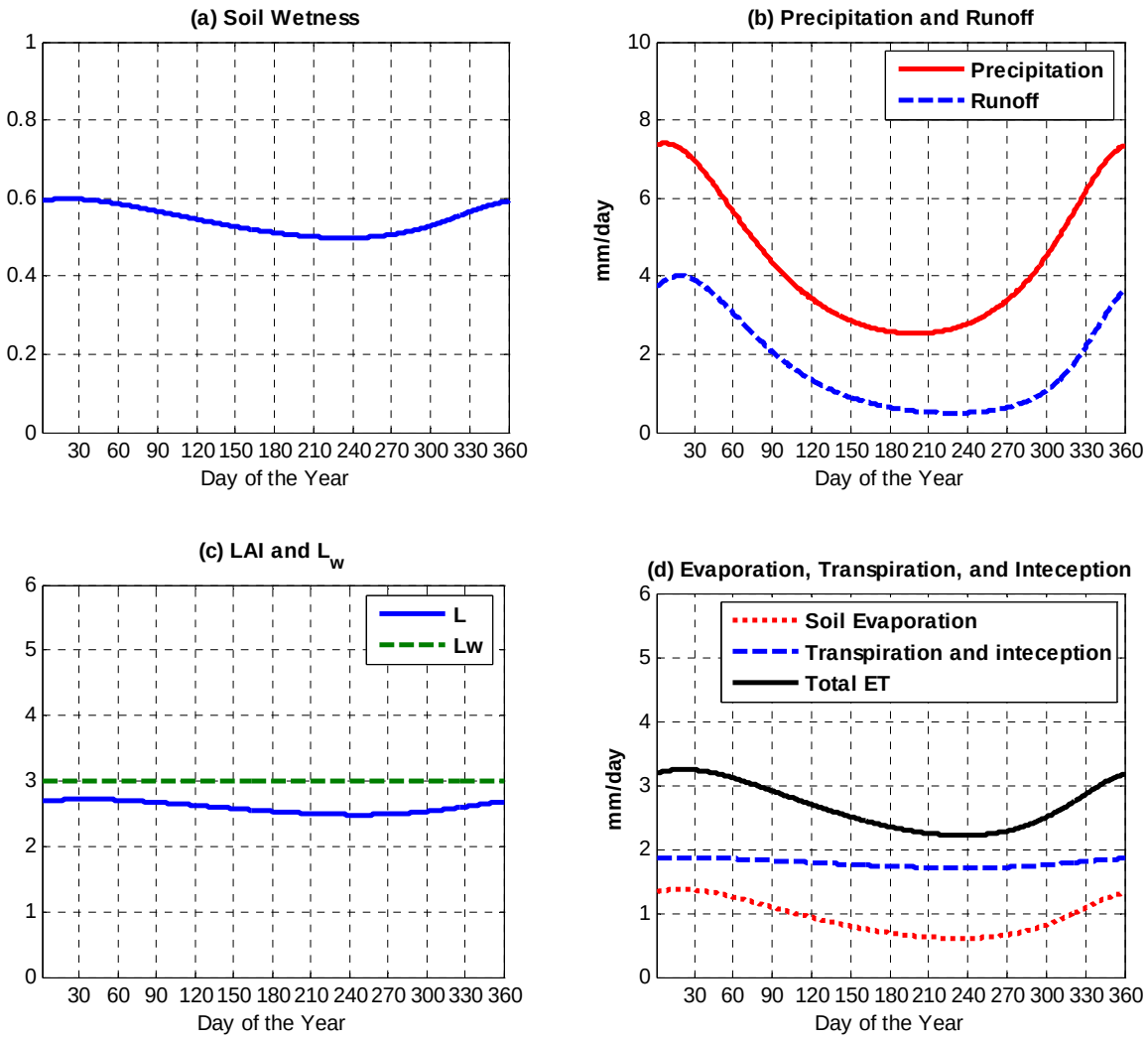

Figure 2.2 Model-simulated seasonal cycles of some variables at no external forcing. L_w is fixed at 3.

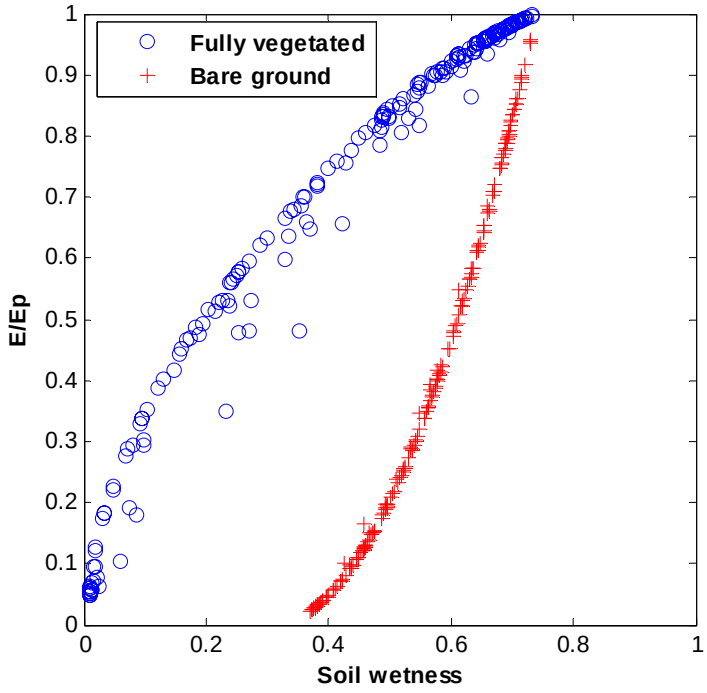

Figure 2.3 ET normalized by its potential value as a function of soil wetness for bare (L_w =0.01) and fully vegetated (L_w =6) land. Monthly average values are shown.

equilibrium while large initial L_ws lead to a wet equilibrium (Figure 2.4a). When we add a weak red noise forcing to the rainfall (forcing strength σ=0.2), the different runs still stay at their dry or wet regime but with some variability (Figure 2.4b). When a stronger noise is added (σ=0.8), the different runs converge to a state between the dry and wet equilibriums, which means that the influence of initial values has disappeared as a result of the forcing of the noise (Figure 2.4c). The stronger the forcing, the faster they converge. This is the mechanism of African Savanna formation talked about in Zeng and Neelin (2000). At the forcing of interannual variability, the desert climate in the north and forest climate in the south converge to an intermediate Savanna climate.

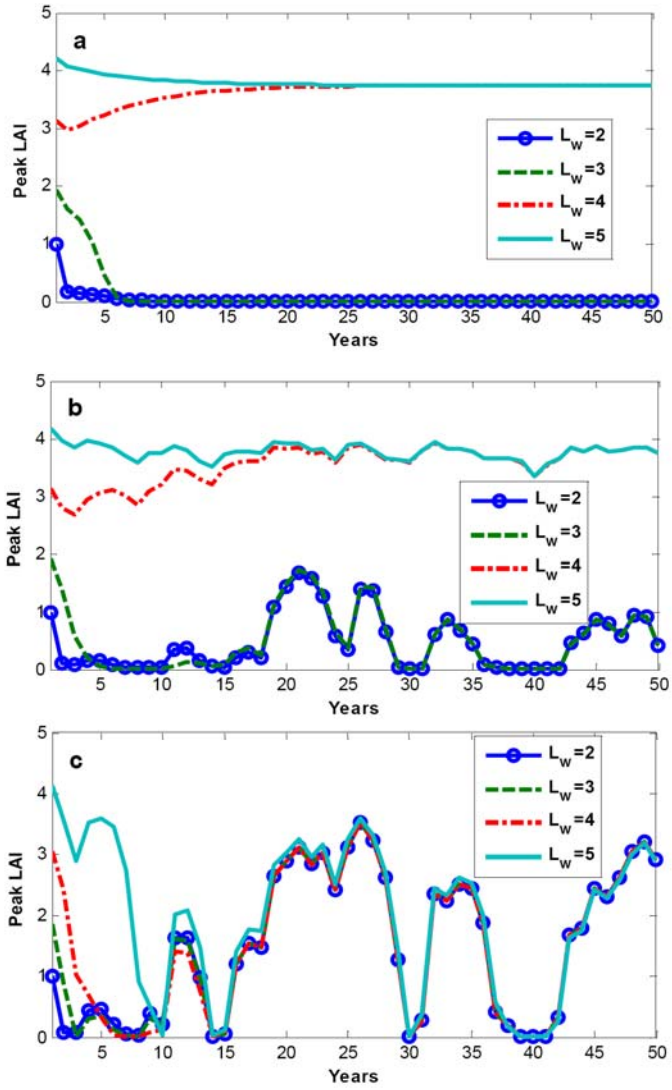

Figure 2.4 Peak LAI from four 50-year model runs with different initial L_w values (shown in legend). (a) without outside forcing, (b) forced by a red noise with forcing strength σ=0.2, and (c) forced by the same noise with forcing strength σ=0.8.

Note that the system does not have multiple-equilibrium states all the time, and it only happens for a certain parameter regime. As this is a coupled model, the change of climate states (dry or wet) can be realized by changing some model parameters, such as the parameters in the formation of precipitation efficiency and recycling ratio (Eqs. 2.15 and 2.16). Figure 2.5 shows how the equilibrium states of the system are determined by $PE_{\min}$, α, and ρ. The parameter space is divided into three regimes. Over two regimes of the parameters, the system has only one stable state: dry or wet; over a certain regime with small minimum PE ($PE_{\min}$) and properly large coupling strength (α) relative to the recycling ratio (ρ), the system has two stable states: dry and wet. Only stable equilibriums can exist in nature. When there is only one stable equilibrium, the equilibrium state is not determined by the initial conditions; when there are two stable equilibriums, different initial conditions can reach totally different equilibrium states, but they can converge to an intermediate state with enough external forcing (Zeng and Neelin, 2000; D'Odorico et al., 2005). The effect of the external forcing is determined by its strength and frequency; our results show that strong low frequency forcing has the most significant effect (not shown). Moreover, catastrophic climate shift (Scheffer et al., 2001) can happen when the change of parameter values makes the climate move from one regime to another. This study shows the equilibrium states of the vegetation-climate system in a two-parameter regime. A similar study in one-parameter regime can be found in Zeng et al. (2004).

These studies have some implications for the regional climate change like in Amazon, Sahel, and Congo basin. How the local climate will change depends not only on the local land use change, but also on the frequency and strength of external forcing (e.g.,

SST and ENSO) and atmospheric internal variability. Enough outside forcing can shift the climate regime between wet and dry.

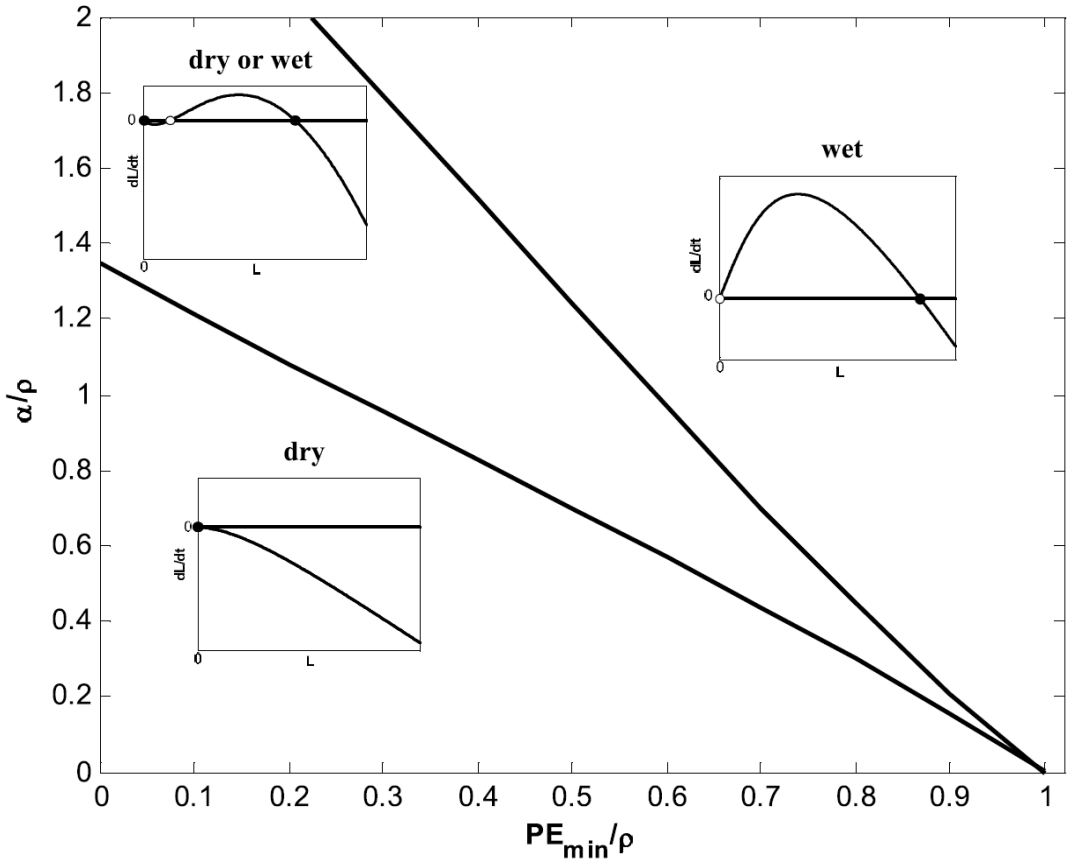

Figure 2.5 The equilibrium states of LAI L in the parameter regime of $PE_{\min}/\rho$ and α/ρ. ρ has no seasonal cycle here. The inserts show the *dL/dt*-*L* relation. The filled circles in the inserts are stable equilibrium states and unfilled circles are unstable equilibrium states. Other hydroclimatological variables such as maximum LAI (L_w), soil wetness (S), and precipitation (P) has similar multi-equilibrium states as LAI.

2.4 Experimental Design

In order to study the land-atmosphere interaction for different land covers and at different external forcings, we performed a series of experiments. As monthly to seasonal climate variability is the focus of this paper, we assume that there is no large vegetation type transition and the L_w values are fixed for each land cover. In the first experiment (Exp1), the L_w values are fixed at 0.5, 2, 3.5, and 5 to represent four different land covers from sparse to dense: desert, grassland, tree-grass mixture and forest. For each land cover, three 50-year runs are performed with external forcing strength σ=2, 0.5, and 0.1, respectively. The second experiment (Exp2) is the same as the first one except that the average seasonal cycles of LAI from the last 40 years of first experiment are used, so there is no interannual variability in LAI, but other variables are still calculated. In the third experiment (Exp3), average seasonal cycles of both LAI and soil wetness from the first experiment are used, so there is no interannual variability in either LAI or soil wetness. The output of the last 40 years of each run is used for analysis. Hence the difference between Exp1 and Exp2 can be regarded as showing the influence of interactive vegetation, and the difference between Exp2 and Exp3 can be regarded as showing the influence of interactive soil wetness.

2.5 Data Analysis Methods

2.5.1 E-folding timescale

Although this is a simple model, it includes substantial nonlinearity and complex interactions. Statistical methods are used to analyze its output variables. The temporal variabilities of the variables are estimated by their autocorrelation. If we assume that the

time series of the variable are similar to a red noise of first-order Markov process (e.g., Delworth and Manabe, 1988), the autocorrelation value can be calculated as (Daniel, 1995)

$$r(t) = \exp(-t/\tau) \tag{18}$$

where τ is the decay time scale, and the autocorrelation r will reach the e-folding value when $t = \tau$. In this study, we use the lag-one-month autocorrelation to calculate τ. The τ value provides a single parameter measure of the memory or persistence of the variables, and can also be used as a measure of predictability. In this paper, the memory, persistence, and predictability all denote the τ values. Note that as the autocorrelation of the hydroclimatological variables in this study decay to insignificant values in one year, the τ value is only a measure of monthly to seasonal variability.

2.5.2 Wavelet and wavelet coherency analysis

As the time series of external forcing contains variations of all kinds of frequencies, the wavelet transform (Torrence and Compo, 1998; Grinsted et al., 2004) is used to analyze it at local time and frequency and its influence on the land-atmosphere interaction. Most traditional methods that examine periodicities in the frequency domain, such as Fourier analysis, have implicitly assumed that the time series are stationary in time and give an average power spectrum for the whole time series. However, most geophysical time series are nonstationary. Wavelet transforms can expand time series into time-frequency space and therefore find localized variability.

In order to examine the coupling between soil wetness and precipitation, the cross-wavelet coherency analysis (Torrence and Compo, 1998; Torrence and Webster,

1999; Grinsted et al., 2004) is used. The cross-wavelet coherency finds regions in time frequency space where the two time series co-vary (in phase or out of phase) but do not necessarily have high power. It is defined as the absolute value squared of the smoothed cross-wavelet spectrum normalized by the smoothed wavelet power spectra. This definition resembles that of the squared correlation coefficient, and it is useful to think of the wavelet coherency as a localized correlation coefficient in time-frequency space. The unique feature of this method is that it measures the local values of both coherency and phase lag of the two time series continuously through time. This feature is overlooked by many other statistical methods, for example, correlation, lagged correlation, and cross spectrum analysis, which describe an average relationship of two time series over a specified time.

2.6 Results

2.6.1 Role of soil moisture and vegetation feedback in climate variability

The τ values for the soil wetness and precipitation anomaly (seasonal cycle removed) time series from the three experiments are shown in Figure 2.6. Generally, soil wetness has larger τ values than precipitation and the τ values of these two variables are larger than that of the noise in Exp1 and Exp2 (Figure 2.6a, b, c, d), which demonstrates the memory of land and its ability to enhance climate predictability. Without the memory from land (both vegetation and soil moisture), the τ values for precipitation in Exp3 are close to the noise (Figure 2.6e). Next, we will compare the results from different land covers and different experiments. Let's look at the results of Exp1 first (Figure 2.6a, b). It evident that when the external forcing is strong (σ=2), the

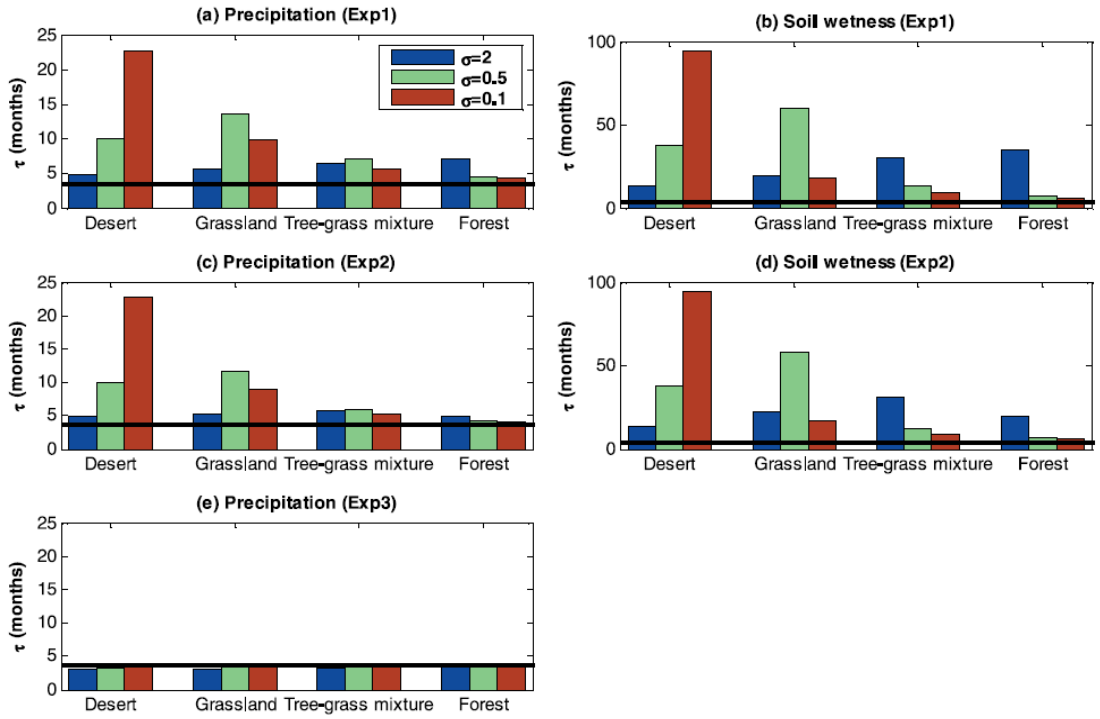

Figure 2.6 The decay time scale τ of monthly soil wetness and precipitation anomaly for different land covers and at different forcing strengths. (a and b) Exp1. (c and d) Exp2. (e) Exp3. The horizontal black line is the τ value of the external forcing. All autocorrelations used to calculate τ values are above the 99% significant level.

τ values at the forest are the largest; with the weakening of the external forcing (σ=0.5, 0.1), the peak τ values move to the grassland and then to the desert. Thus the peak τ values tend to move from dense to sparse vegetation covers with the weakening of the external forcing. That is, a dense vegetation cover, with its large resilience, will take a long time to recover from a dry or wet anomaly caused by a strong external forcing, while if the external forcing is weak the internal interactions in the land-atmosphere system will induce some high-frequency variability relative to the average state, although in smaller amplitude than that from a stronger forcing, and decrease the climate

persistence. On the contrary, a sparse vegetation cover has little memory and is more responsive to a strong forcing, hence the memory and τ values will be smaller with a strong forcing. In Exp2, after we fix the LAI to the seasonal climatologies, the τ values for a certain forcing decrease over the vegetated land and have little change over desert (Figure 2.6c, d). The reason is that climate-vegetation interaction can damp the high frequency climate variability and increase the climate persistence (Zeng et al., 1999; Wang and Eltahir, 2000c).

If we assume that the contributions of interactive soil wetness and interactive vegetation to the τ values linearly add, we can analyze their respective contributions from the τ value differences of the three experiments (Figure 2.7). Three different forcing strengths: weak, medium, and strong (σ=0.1, 0.5, and 2) are added to the precipitation. It is found that soil wetness contributes more to the predictability than vegetation over almost all the land covers (except forest at strong forcing), and that the contribution of vegetation is much smaller over sparse vegetation covers and comparable only at dense vegetation covers; the percentage of contribution from interactive vegetation increases with vegetation density.

Of the three forcing strengths for the precipitation, medium forcing (σ=0.5) is most realistic (as can be judged from the signal-to-noise ratio), so its τ values as measuring precipitation predictability are most close to the current climate and can be compared with other studies. At the medium forcing, the contribution of soil wetness to the predictability is largest at the grassland, which is consistent with previous GCM results that soil moisture contributes most to precipitation predictability in transitional zones between dry and humid climates (Koster et al., 2000, 2004). The contribution of

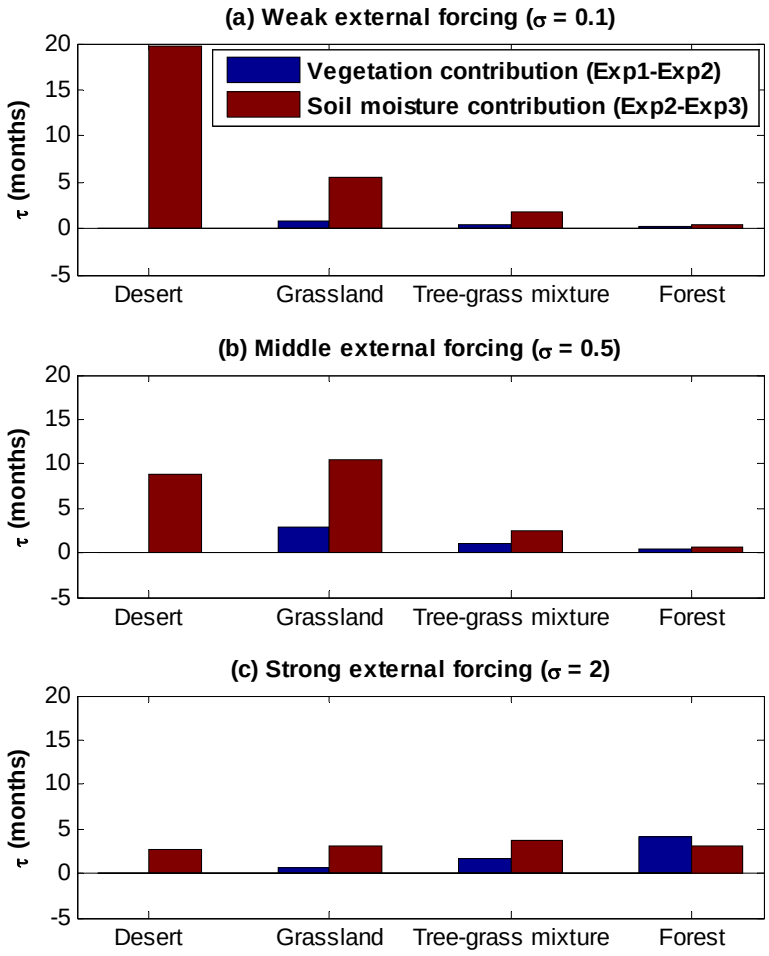

Figure 2.7 The τ value difference of precipitation at different forcing strengths and for different land covers. Blue bars are for Exp1-Exp2, which is the contribution of interactive vegetation to the precipitation predictability; red bars are for Exp2-Exp3, which is the contribution of soil wetness to the precipitation predictability.

interactive vegetation is largest over the tree-grass mixture and grassland and is reduced over forest by the large resilience and saturation effects. However, the maximum contributions of soil wetness and interactive vegetation move to a denser (sparser) vegetation cover with the strengthening (weakening) of external forcing (Figure 2.7a, c). Although the weak and strong forcings (σ=0.1 and 2) may be too weak and too strong and not realistic, they still indicate that the region of strongest land influence may have some slight interannual variation with the interannual variation of climate This also indicates that the "hot spots" of land-atmosphere interaction suggested by Koster et al. (2000, 2004) may move in a future climate change.

2.6.2 Role of vegetation and external forcing in soil moisture-precipitation relation

The cross-wavelet coherency between soil wetness and precipitation for Exp1 and Exp2 at forcing strength σ=0.5 is shown in Figure 2.8. In general, there is more coherency at low-frequencies than at high frequencies because the soil moisture and precipitation correlates better at longer timescales. The vegetated lands have less low-frequency coherency than desert for both experiments because of vegetation shading, interception and soil-vegetation-atmosphere interaction. With the vegetation fixed at seasonal climatologies, Exp2 shows almost the same coherency pattern as Exp1 except that the coherency is weakened in some low-frequency regime due to lack of vegetation interaction (Figure 2.8f). This weakening illustrates that the interactive vegetation may enhance the low-frequency soil wetness-precipitation coherency. In addition, as talked about above, the influence of interactive vegetation depends on the strength of external forcing, and the maximum influence (figure 2.8f) may move to denser vegetation with the

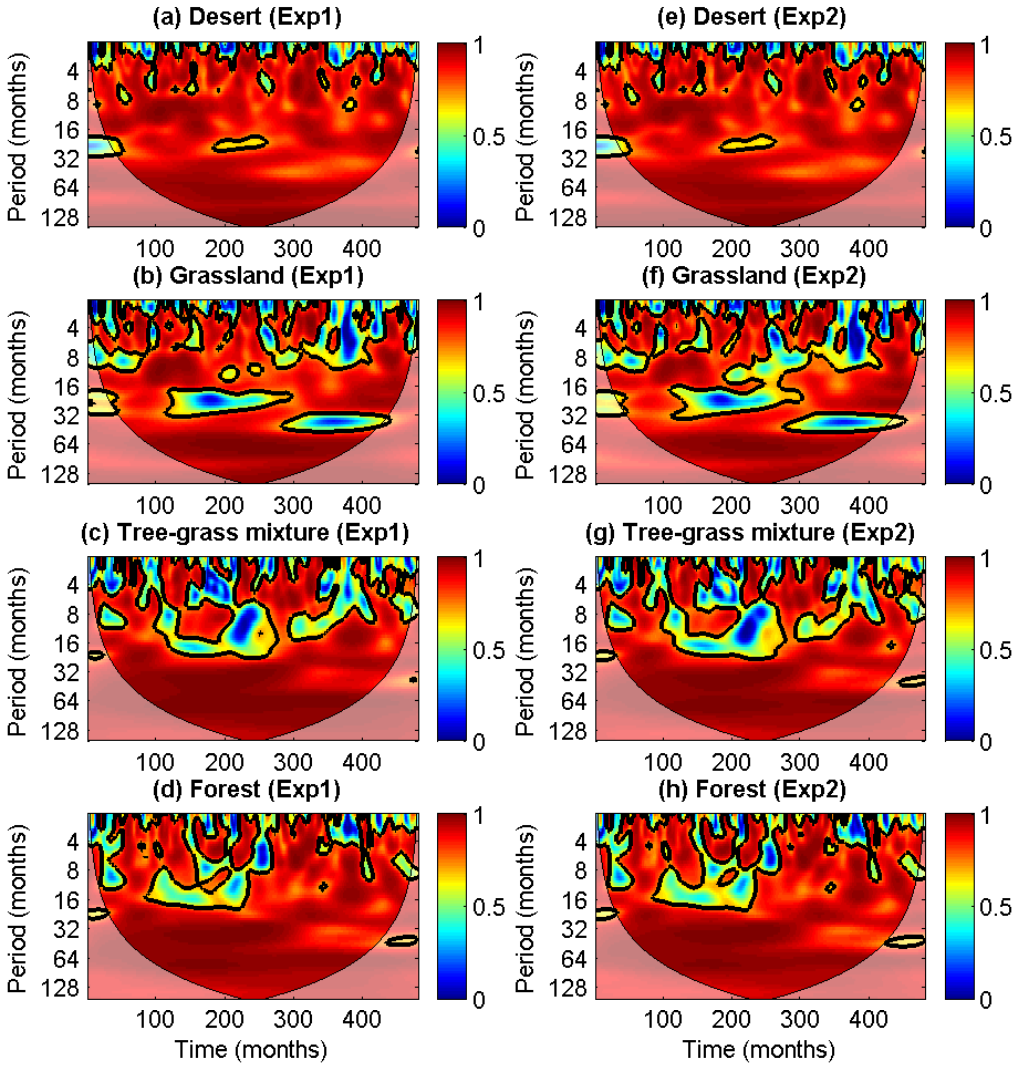

Figure 2.8 Cross-wavelet coherency between soil wetness and precipitation anomalies for different land covers. Forcing strength σ=0.5. (a, b, c, and d) Exp1. (e, f, g, and h) Exp2. The thick black contour is 5% significance level against red noise, and the cone of influence where edge effects might distort the picture is shown as a lighter shade. The phase information is not shown in this figure. Generally, precipitation leads soil wetness about 1/8 period at periods less than 1 year and is in phase with soil wetness at periods larger than 1 year.

strengthening of the forcing (not shown). Due to the complex nonlinear interactions in the model, the coherency patterns vary nonlinearly with the forcing strength (not shown), but several weak coherency centers exist regardless of the forcing strengths, such as the weak centers around (50, 8), (200, 0-4), (200, 16-32), (380, 0-4), and (420, 0-4) (Figure 2.8).

In order to further investigate the relationship between the coherency and external forcing, we compare the coherency pattern with the wavelet power spectrum of the forcing time series (F) in the same time-frequency domain (Figure 2.8 and 2.9). It is found that the weak coherency centers in Figure 2.8a and e (as listed above) correspond very well to the weak power centers in Figure 2.9 for both high and low frequencies. We only compare the coherency centers appear at desert because they may be amplified or slightly moved by stronger vegetation influence at other land covers. Evidently, this good correspondence indicates that much of the large coherency between soil wetness and precipitation is due to the strong external forcing, and during periods of weak forcing the coherency will be small. This corresponds to a "threshold effect" as suggested by Oglesby et al. (2002): a strong external forcing can induce a large soil wetness anomaly, which can lead to a strong feedback that make precipitation and soil wetness vary in the same direction; while if the external forcing is weak the precipitation and soil wetness anomalies will be small, and the coherency will be weakened by the variability of atmospheric and land processes.

As the parameterization of precipitation is a very uncertain part of our model, and a slight change of the parameter values may, as mentioned in chapter 2.3, lead to completely different equilibrium states, some experiments are performed with a little different $PE_{\min}$ and α values, different formation of equation (2.16), and different noise.

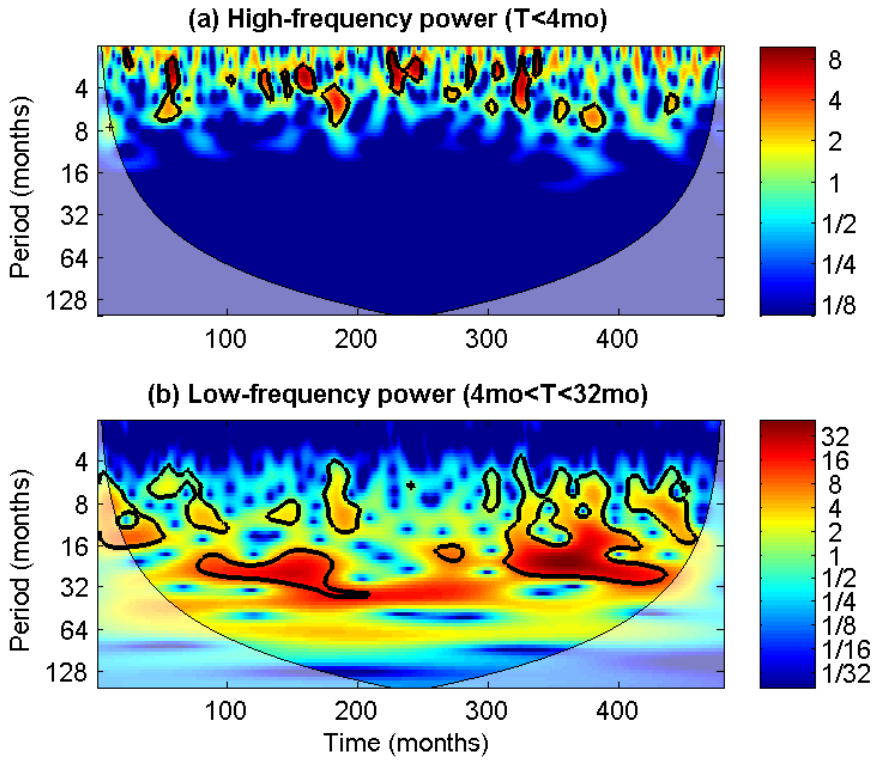

Figure 2.9 The continuous wavelet power spectrum of the external forcing. (a) high-frequency power (period T<4 months). (b) low-frequency power (4 months<T<32 months). The thick black contour is 5% significance level against red noise, and the cone of influence where edge effects might distort the picture is shown as a lighter shade.

No qualitative change is found in the results except that the positions of peak τ values in Figure 2.6 may move with climate change.

We have shown some relationships found with the simple model. Next, we will look at some realistic data to see whether such relationships really exist in nature. The 10-year monthly GSWP-2 data (see section 3.2.2) is used to show the S-P coherency (same as Figure 2.8) and wavelet transform of precipitation (same as Figure 2.9 but for precipitation) in Figure 2.10. The wavelet of precipitation, but not of the forcing as in the

model, is used because the forcing is hard to be estimated from realistic data. Precipitation variability is close enough to the forcing variability. Two regions with warm climate for the whole year are selected: the Sahel and the Amazon basin. Sahel represents a region with sparse vegetation, while Amazon basin represents a region with dense

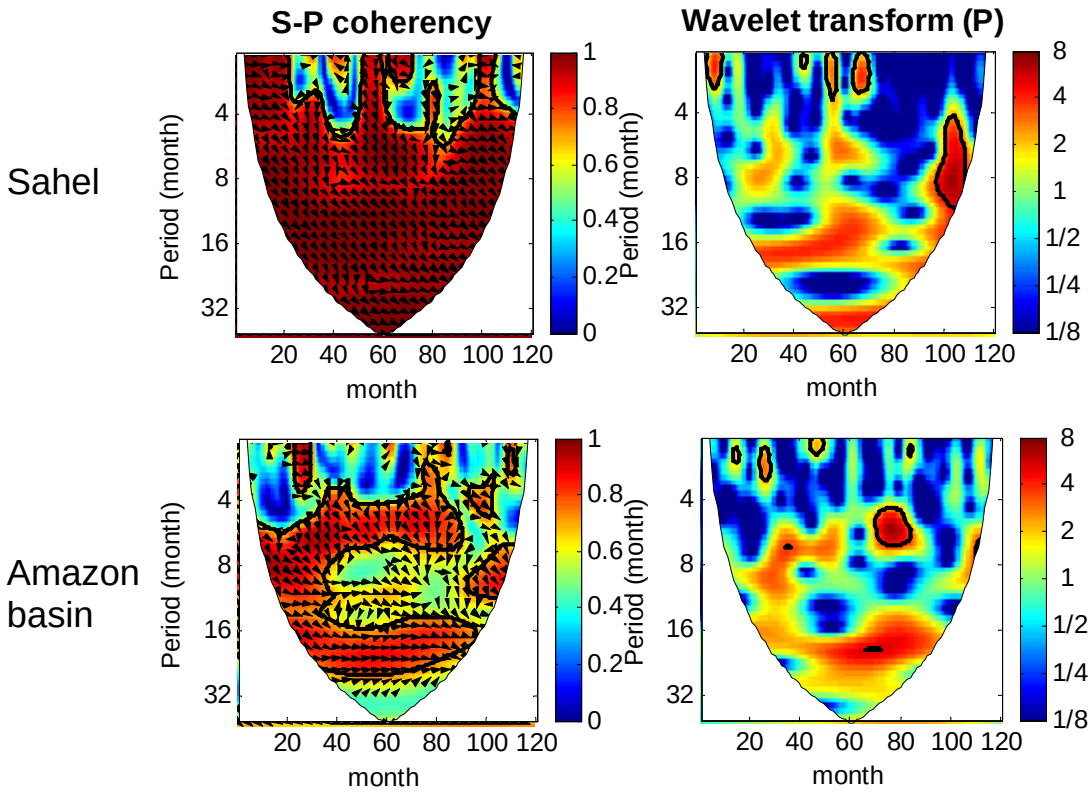

Figure 2.10 S-P coherency and wavelet transform of precipitation calculated from 10-year monthly GSWP-2 data. The left column is S-P coherency and the right column is wavelet transform of precipitation. The upper row is for Sahel and the bottom row is for Amazon basin. The arrows in the coherency figures indicate the phase relation of soil moisture and precipitation. Generally, precipitation leads soil wetness about 1/4 period at periods less than 1 year and is in phase with soil wetness at periods larger than 1 year.

vegetation. It can be seen in Figure 2.10 that the Sahel has more low-frequency coherency than the Amazon basin because of less influence from interactive vegetation. The weak centers of S-P coherency correspond well to the weak center of the wavelet transform of precipitation. These results are consistent with the model results.

2.7 Conclusions and Discussion

This study develops a simple model of warm climate land-atmosphere interaction with interactive land components – soil wetness and vegetation. Because of its simplicity, such a model is useful for many applications; for example, it can be easily integrated for a long time to estimate the trend of climate variation, it can clearly separate variability from different sources and analyze their individual influence on climate variability, and different climate conditions can be easily represented by changing a few model parameters. However, its simplicity may lead to difficulties; it has no variability from energy balance or related processes, no boundary layer processes, and no atmospheric dynamics. Although these limitations may reduce the applicability of this model, it is especially suitable for study of climate variability on seasonal to decadal timescales and can provide some guidance for GCM study.

The model is used to study the role of land surface processes in climate variability over different land covers and at different external forcings. The major findings and their implications for the current model studies on warm climate land-atmosphere interaction and climate prediction are:

1) The decay time scales of soil wetness and precipitation maximize at sparser (denser) vegetation covers with the weakening (strengthening) of external forcing. Hence both

the strength of external variabilities and the regional land cover influence the soil moisture and precipitation persistence. In a model, these external variabilities can come from natural regional climate variability or incorrect model internal dynamics. These incorrect variabilities in the model may act on the simulated soil moisture and precipitation persistence and even transfer to other component in the climate system (e.g., Wang and Eltahir, 2000b). Therefore, accurate simulation of climate variability besides mean climate is an urgent task facing model developers.

2) The persistence of soil wetness and precipitation is larger with interactive vegetation, if it is dense, and changes little, if vegetation is sparse. Thus fixing vegetation in a model may underestimate the soil moisture memory and precipitation predictability for densely vegetated warm regions. Interactive vegetation in these regions is necessary if a good estimate of soil moisture memory and precipitation predictability is desired.

3) Interactive vegetation can enhance the low-frequency coherency between soil wetness and precipitation at some land covers (depending on the forcing), but its influence on high-frequency coherency is small. Thus fixed seasonal vegetation will not have much influence on the soil wetness-precipitation relationship at monthly to seasonal timescales. It also appears that interactive soil moisture is more important than interactive vegetation for precipitation variation at these timescales. This is due to the different ways soil moisture and vegetation interacts with the atmosphere. Observational data also shows that the local vegetation feedback has little influence on precipitation at monthly to seasonal timescales and the influence is larger at a

longer timescale (Liu et al., 2006) when the vegetation succession plays an important role (Zeng et al., 1999).

4) A strong external forcing can induce a large soil wetness anomaly and a large coherency between soil wetness and precipitation, while such coherency may be weak if the external forcing is weak. The coherency here shows the lagged correlation between soil moisture and precipitation, with soil moisture lags precipitation at monthly to seasonal time scales (Figure 2.8 notation) because soil moisture integrates the influence of past precipitation while the influence of soil moisture feedback on future precipitation is smaller than the natural variability of precipitation (see chapter 3). Our study on their coherency shows that their relationship depends on the strength of external forcing; a strong external forcing at a certain time and frequency can induce a strong coherency (simultaneous or lagged relationship) between soil moisture and precipitation at a corresponding time and frequency. As external forcing is usually nonstationary, their relationship and coherency also exhibit an on-and-off feature.

In this study, the influence of local land processes on precipitation predictability is divided into the contribution from soil wetness and the contribution from interactive vegetation. This influence can also be divided into the contribution from ET and the contribution from PE (Eq. 2.15). In order to study their relative importance, two additional experiments are performed with ET or PE fixed at seasonal climatologies of Exp1 to neglect their interannual variabilities. They are denoted Exp4 and Exp5, respectively. By comparing the τ value difference for precipitation between these two experiments and fully interactive Exp1, we can obtain the contribution of ET and PE to

the precipitation predictability, respectively. Figure 2.11 shows that both ET and PE can contribute to the precipitation predictability, but that the contribution of ET is much larger. The reason may be that there is no seasonal temperature variation in the warm climate we assumed. As PE is mainly controlled by the monthly temperature, its changes will be small, while ET, which is mainly controlled by surface soil wetness and vegetation, will have a relatively large change. Thus fixing ET at seasonal climatologies will decrease its control on precipitation and the precipitation variability will mainly come from external forcing with little predictability, while fixing PE at seasonal climatologies has a relative small influence on the precipitation predictability. In this sense, ET is more important than PE in the warm climate seasonal precipitation prediction.

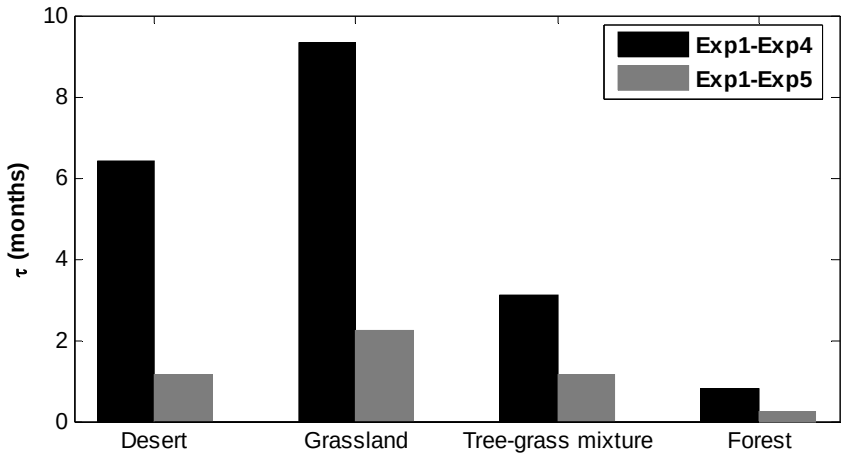

Figure 2.11 The τ value difference of precipitation for different land covers. Forcing strength σ=0.5. Dark bars are for Exp1-Exp4, which is the contribution of ET to the precipitation predictability; bright bars are for Exp1-Exp5, which is the contribution of PE to the predictability.

A major simplification of the model is its neglect of atmospheric dynamics and ocean interaction. Although the red component of the added forcing is similar to the persistence of the atmosphere and ocean, the linear precipitation parameterization neglects the possible scale interactions in the climate system, such as the interactions between tropical convection, Madden-Julian oscillation, and ENSO. This neglect may be the reason the weak coherency centers between soil wetness and precipitation corresponds so well to the weak wavelet power centers of external forcing in the time-frequency domain. Hence these result needs to be examined by coupled nonlinear models.

This model provides a framework for revision or further development as needed. The precipitation and vegetation parameterizations of the model are designed for warm climate with convective precipitation. With more feedbacks from temperature, radiation, and chaotic atmospheric dynamics, the land-atmosphere interaction processes in cooler climate will be more complex, but their study may be guided by the results attained here.

CHAPTER 3

A SOIL MOISTURE-PRECIPITATION RELATION IN REANALYSES AND MODELS

3.1 Background

The interaction between soil moisture and precipitation is a very important question in land-atmosphere interaction. The main soil moisture-precipitation (S-P) interaction process is cyclic as follows: precipitation falls to the ground and wets the soil, and with the forcing of solar radiation soil water evaporates or transported by vegetation to the atmosphere; some of this water vapor is transported to other places and some, together with water vapor arriving from elsewhere, forms precipitation. Due to the lack of large scale observations and very limited local observations many processes in the S-P interaction are still not well understood. Analyses of the limited local soil moisture and precipitation data even lead to contradictory interpretations: some have demonstrated that soil moisture have a significant influence on subsequent precipitation (e.g., in Illinois; Findell and Eltahir 1997), but some, with the same data, have argued that soil moisture does not have a significant influence on precipitation (e.g., Salvucci et al. 2002).

Modeling can provide more comprehensive data and the capability to analyze causality, so it is still a major method in current study. By analyzing the model results from Global Land–Atmosphere Coupling Experiment (GLACE; Koster et al. 2004, 2006), Guo et al. (2006) separated the ability of soil moisture to affect precipitation into the ability of soil moisture to affect evaporation and the ability of evaporation to affect precipitation. They found that most of the differences between models and within a given

model are found to be associated with the first part. Ruiz-Barradas and Nigam (2005, 2006) examined the summer hydroclimate variability of North American in reanalyses and models. They found that there are large discrepancies among the datasets on the relative contributions of remote and local water sources to the Great Plains precipitation, and in particular, that the stationary moisture flux contributes most in ERA-40 and North American Regional Analysis (NARR), but not in NCEP reanalysis and model simulations.

After several decades of development, climate models can now simulate many observed climate phenomena, such as seasonal to decadal climate variability, but many detailed aspects still cannot be reproduced (e.g., Dirmeyer et al. 2006a). If we are going to use a model to the study the feedback processes of a climate phenomenon, the model should first be able to reproduce the climate phenomenon properly. However, for land-atmosphere interaction study, model evaluation becomes especially difficult because of the paucity of large-scale land observations. In this study, three different reanalysis products and the data from Global Soil Wetness Project Phase 2 (GSWP-2; Dirmeyer et al. 2006b) are used for comparison and model evaluation. Although the land data from them are also not observed, they are produced from model simulations that are highly constrained from observations and have a higher credibility than model simulations that are not so constrained.

The aim of this study is not to provide an evidence of soil moisture variations affecting precipitation, as has been studied by Koster et al. (2003), and is also not to search for the regions where soil moisture variations have significant influence on precipitation, as is the purpose of GLACE. This study explores an S-P relationship that

commonly exits in reanalyses and models and tries to understand the causes of it. We first compared an S-P correlation in reanalyses and GSWP2 data, and their consistency is set as a benchmark to be compared with CAM3 simulations. Carefully designed experiments with CAM3 show that soil moisture feedback plays little role in this S-P correlation pattern. The mechanisms that cause this relation are discussed.

3.2 Datasets

3.2.1 Reanalyses

Three reanalysis products are used for this analysis: the ERA-40 (Uppala et al. 2005) from ECMWF, the NCEP-DOE reanalysis 2 (R-2; Kanamitsu et al. 2002), and North American Regional Reanalysis (NARR; Mesinger et al. 2006). ERA-40 is a second-generation reanalysis carried out after the successful ERA-15 (Gibson et al. 1997). ERA-40 uses a land scheme to model surface exchanges (Van den Hurk et al. 2000). The surface fluxes in a grid box are calculated separately for different subgrid fractions (or "tiles"), leading to a separate solution of the surface energy balance equation and skin temperature for each of these tiles. There are 18 vegetation types based on BATS (Dickinson et al. 1993), and the land surface parameters vary per vegetation type. R-2 is an update of the widely used NCEP/NCAR reanalysis (R-1; Kalnay et al. 1996). R-2 has newer physics and eliminates several previous errors in R-1. As in R-1, R-2 uses a simple land surface model (Mahrt and Pan 1984; Pan and Mahrt 1987; Pan 1990). Vegetation and surface characteristics are from the SiB climatology (Dorman and Sellers 1989). The ERA-40 and R-2 use different nudging techniques to correct soil moisture drift caused by imperfect precipitation and insolation (see Li et al. 2005 for a summary).

The NARR project is an extension of the NCEP Global Reanalysis for the North American domain. The NARR model uses the very high resolution NCEP Eta Model together with the Regional Data Assimilation System (RDAS) which significantly assimilates high-quality and detailed precipitation observations. As a consequence, the forcing to the land model is more accurate than that of previous reanalyses, so that NARR provides a much-improved analysis of land hydrology and land-atmosphere interaction. The lateral boundary conditions for NARR are from R-2. The land model is a recent version of Noah land-surface model (Ek et al. 2003).

3.2.2 Global Soil Wetness Project Phase 2 (GSWP-2)

The 10-year (1986-1995) data from GSWP-2 (Dirmeyer et al. 2006b) is also used for comparison. GSWP-2 combines the simulations of 13 land surface models using the same observation based external forcing and standardized soil and vegetation distributions. The process of averaging across models is found to contribute greatly to the quality of the estimates, as compared to the individual models (Gao and Dirmeyer, 2006).

3.2.3 Details of datasets

The temporal coverage, spatial resolution, and soil-layer thicknesses of the three reanalysis products and GSWP-2 data are shown in Table 3.1. The top 2 m soil moisture is used for analysis. An exception is GSWP-2, which has only 1.5 m of soil moisture data available. The 24 years (1979-2002; 10 years for GSWP-2) of data are used for analysis. The soil water of top 2 m but not the usually used top 1 m is used for two reasons: (1) some products (e.g., R-2) do not have soil moisture of top 1 m; and (2) our study focuses

on the S-P interaction on a relatively long time scale, which may be related to soil water in deeper layers. In fact, after removing the seasonal climatology the soil moisture anomalies at 1 m and 2 m differ very little because most of the soil moisture variations are near the surface.

Table 3.1 The temporal coverage, resolution, and soil-layer thicknesses of the datasets.

	temporal coverage	spatial resolution	soil-layer thicknesses (from top to bottom)
ERA-40	Sep. 1957 to Aug. 2002	2.5ºx2.5º	7, 21, 72, and 189cm
R-2	Jan. 1979 to Dec. 2005	T62 (~1.875ºx1.9º)	10 and 190cm
NARR	Jan. 1979 to present	32km (~0.3º)	10, 30, 60, and 100cm
GSWP-2	Jan. 1986 to Dec. 1995	1ºx1º	150cm (only one available now)

3.3 Preliminary comparison of datasets

Figure 3.1 shows the daily soil water of the top 2 m at Illinois from three reanalysis products, GSWP-2, and observational data from Illinois State Water Survey (Hollinger and Isard 1994; Robock et al. 2000). NARR and GSWP-2 have larger amplitude of seasonal variation, and their mean values are closer to the observations (Figure 3.1a). ERA-40 and R-2 have lower mean values and smaller amplitude of

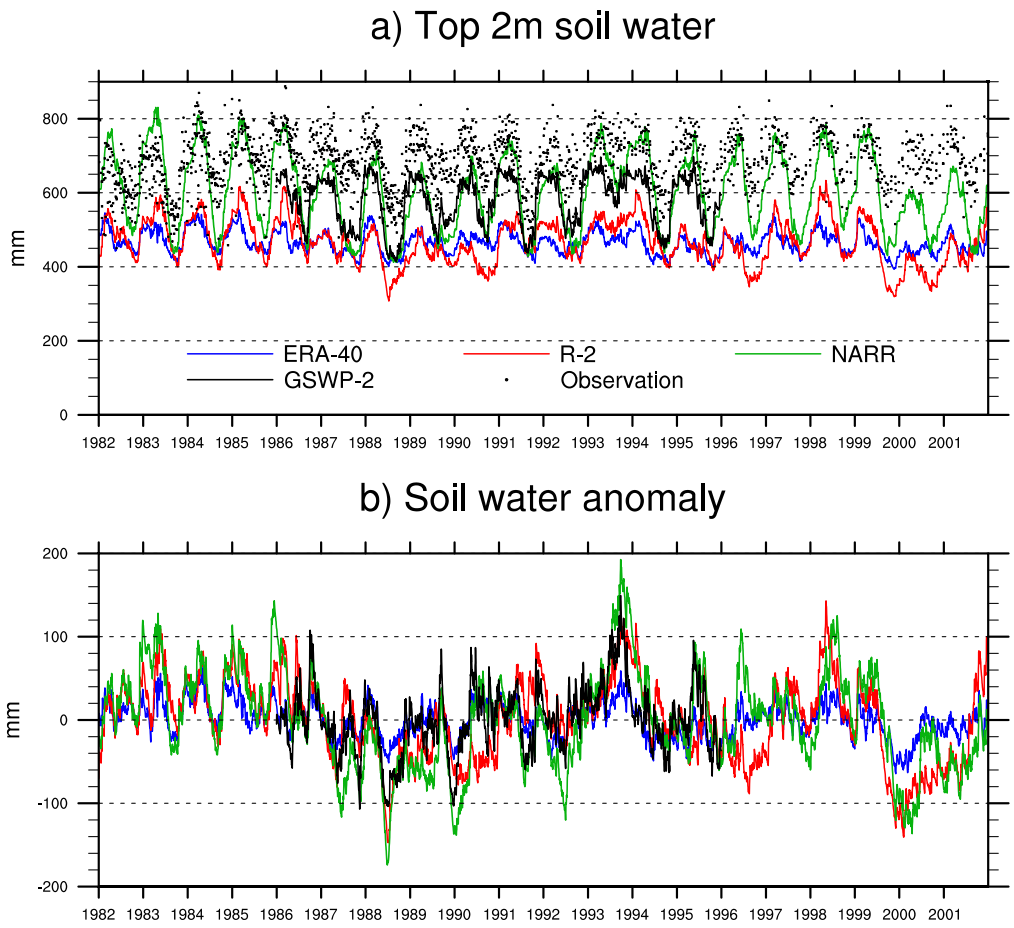

Figure 3.1 Daily soil water of the top 2 m at Illinois from ERA-40, R-2, NARR, GSWP-2, and observational data. (a) Soil water. (b) Soil water anomaly after removing the seasonal cycles. The GSWP-2 data is multiplied by a factor of 4/3 to normalize its 1.5 m soil water to the 2 m of the other datasets.

seasonal variation. After removing their respective seasonal climatology, the different time series show more similarity (Figure 3.1b). The correlations between the three anomaly time series are 0.65-0.73. Although NARR and GSWP-2 still have larger amplitudes, these are not so evident as in the original time series. The 1988 drought and 1993 flood stand out even more than in the original time series. The anomaly time series are more physically relevant as different models and observations can have different values of unavailable soil moisture, which is determined by parameters of soil properties, vegetation rooting depth etc. The anomaly time series is used for the next calculation.

The correlations of some hydroclimate variables between ERA-40 and R-2 are shown in Figure 3.2. Soil water has a stronger correlation than that of precipitation and ET. The correlation of downward solar radiation at the surface is the best, with all the values close to 1 and only a few smaller values in the tropics. If we take the solar radiation as an external forcing to the climate system, this similar forcing in the two reanalyses causes different hydroclimate variabilities, with soil water having a better correlation than that of precipitation and ET. There are two reasons I can think of for this. Firstly, soil water variation is a slow process and has higher predictability than the faster precipitation and ET processes. Secondly, the two reanalysis product both used some kind of nudging techniques for soil moisture to prevent it from drifting too far away from reality.

Although GSWP-2 only has 10 years of data, it integrates land surface outputs from different land models forced by the best atmospheric data available and is proven to be better than any individual model. The precipitation forcing data of GSWP-2 is a hybrid of reanalysis, observations, and empirical corrections (Zhao and Dirmeyer 2003).

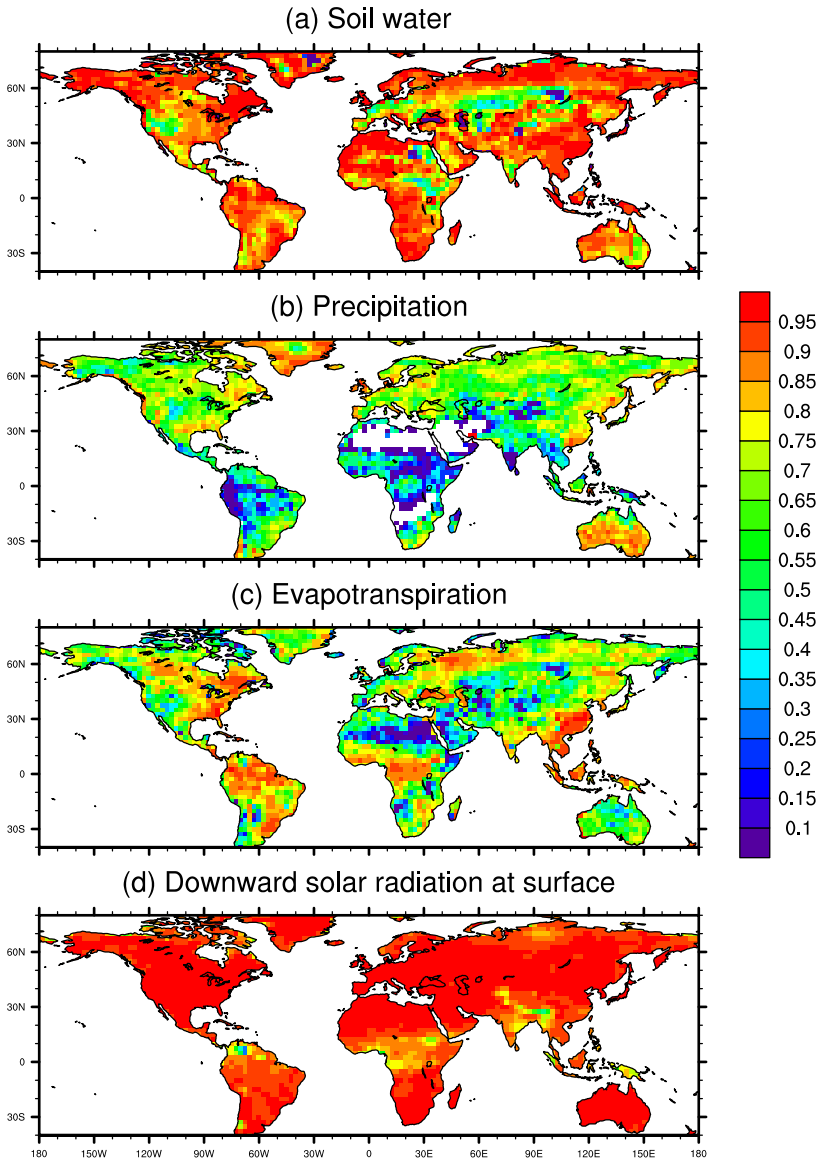

Figure 3.2 The summer (JJA) monthly anomaly correlations of (a) soil water of top 2 m, (b) total precipitation, (c) ET, and (d) downward solar radiation between ERA-40 and R-2. R-2 data is interpolated to the same grid as ERA-40.

The soil water and convective precipitation correlations between GSWP-2 and two reanalyses are shown in Figure 3.3. Soil water still has a better correlation than that of precipitation for both ERA-40 and R-2. GSWP-2 has much better soil water correlation with ERA-40 than with R-2. Their correlations of convective precipitation are similar, i.e., neither one is much better.

NARR mainly covers the North America region. Its direct assimilation of observed precipitation makes the precipitation field very realistic. The land surface variables and other meteorological fields also benefit from the realistic precipitation forcing. The correlations between NARR and ERA-40, R-2, and GSWP-2 are shown in Figure 3.4.

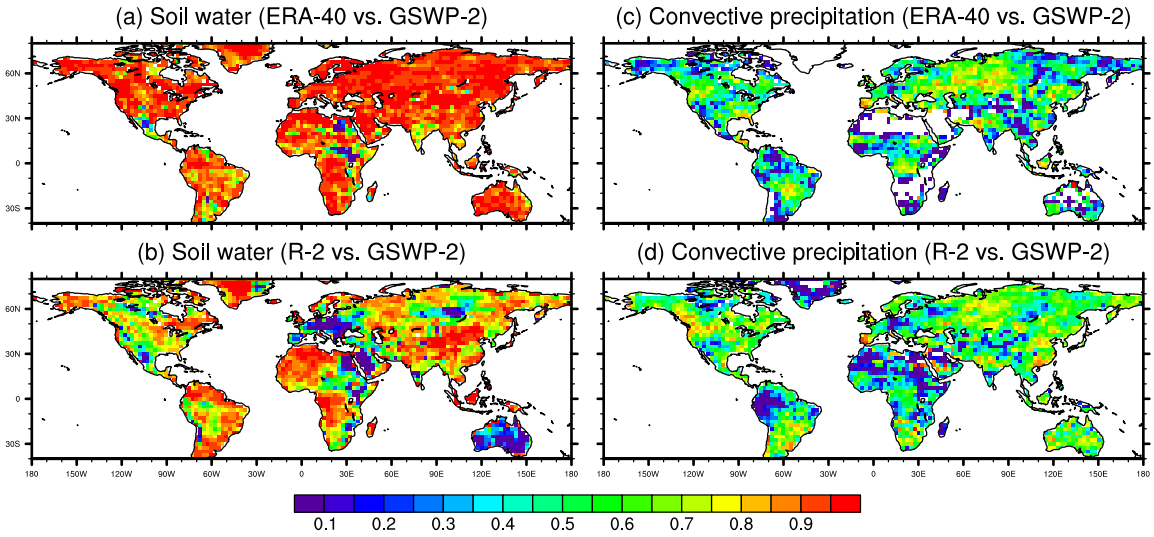

Figure 3.3 The summer (JJA) monthly anomaly correlations of soil water at top 2 m (left column) and convective precipitation (right column) between ERA-40 and GSWP-2 (upper row) and R-2 and GSWP-2 (lower row). R-2 and GSWP-2 data is interpolated to the same grid as ERA-40.

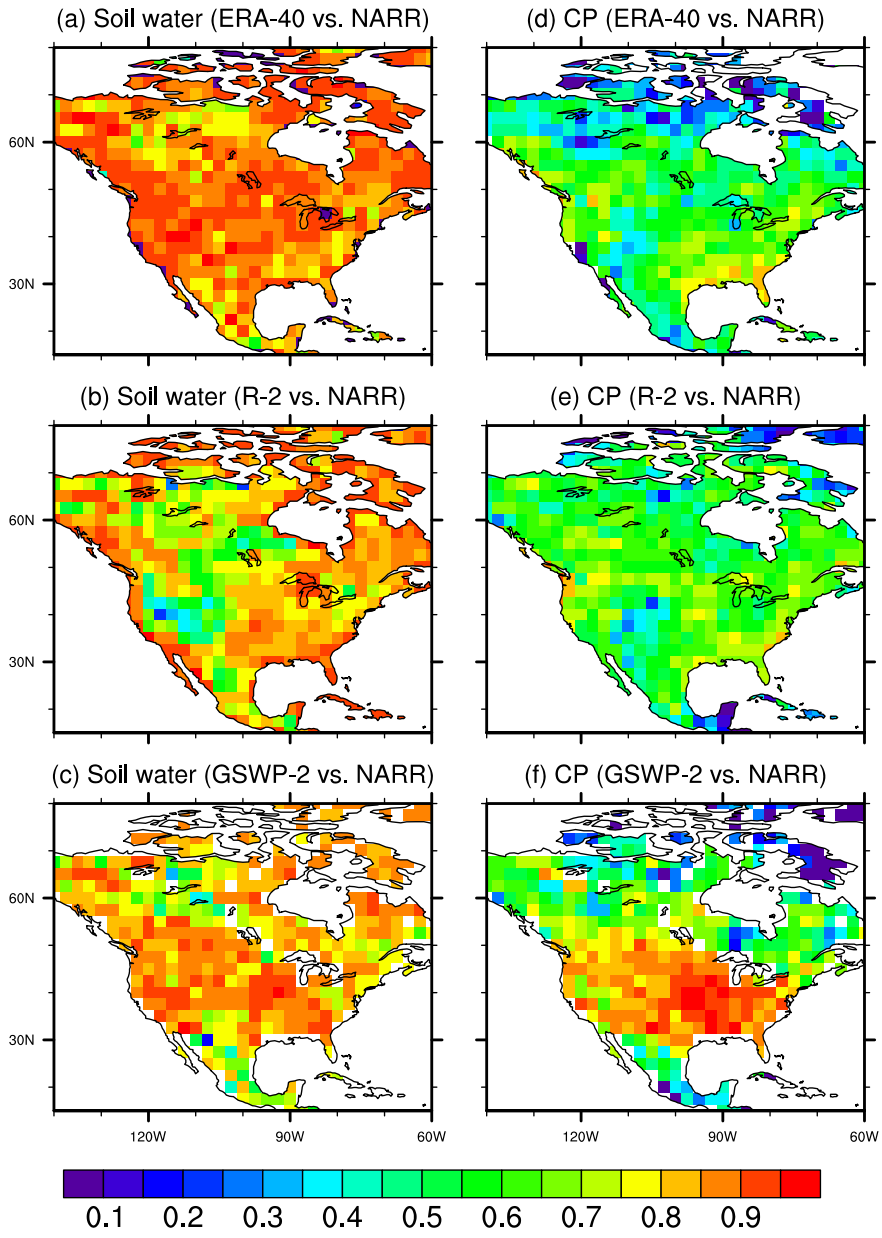

Figure 3.4 Same as Figure 3.3, but between ERA-40 and NARR (top row), R-2 and NARR (middle row), and GSWP-2 and NARR (bottom row). All the data is interpolated to the same grid as ERA-40.

ERA-40 and GSWP-2 has better soil water correlation with NARR than that of R-2. The convective precipitation from GSWP-2 has a much better correlation with NARR than with ERA-40 and R-2, especially in the United States, an obvious result of the realistic assimilation of precipitation in NARR and the realistic precipitation forcing of GSWP-2.

For the reasons mentioned above, we are inclined to set GSWP-2 and NARR as the benchmark for comparison. From the above analysis we can find that ERA-40 has better soil water variability than that of R-2 when compared with GSWP-2 or NARR. The weakness of R-2 is mainly in East Africa, Arabia, Europe, Siberia, Australia, and Western United States. As for the precipitation variability, ERA-40 and R-2 both has some discrepancies with observation based GSWP-2 and NARR. The discrepancies between ERA-40 and R-2 are mainly in the regions with a sparse distribution of observational stations (Figure 3.2b).

In Figure 3.3-3.4, we focused on comparing the convective precipitation because it is more related to local processes, which are the focus of this study. Although the summer precipitation is mainly convective, the proportion of convective precipitation in the total precipitation differs among the different data sets (Figure 3.5). ERA-40 has the lowest proportion of summer convective precipitation, and R-2 and GSWP-2 have the highest. The pattern of GSWP-2 is very close to that of R-2. NARR data in North America shows a percentage of convective precipitation between ERA-40 and R-2/GSWP-2.

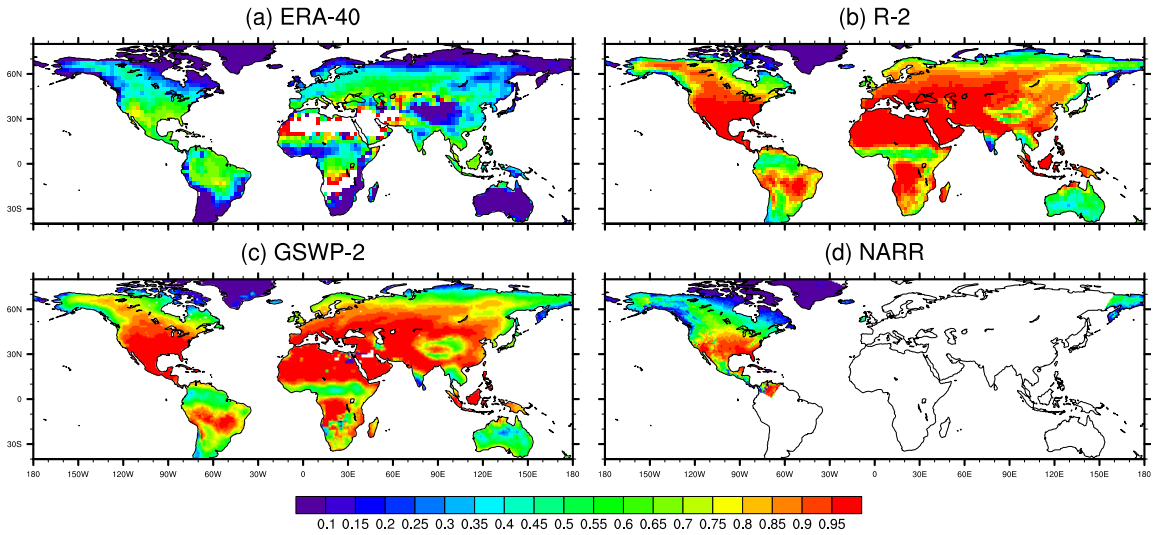

Figure 3.5 The summer percentage of convective precipitation in the total precipitation for (a) ERA-40, (b) R-2, (c) GSWP-2, and (d) NARR datasets.

3.4 S-P relations in different datasets and CAM3

3.4.1 Calculation method

There are 92 summer days (June 1 to August 31) in each year. For the first 62 days (June 1 to August 1), the soil water of the top 2 m in each day is put in a time series, and the total precipitation in each subsequent 30 days (June 2 to July 1, June 3 to July 2, …, August 2 to August 31) is calculated and put in another time series. The correlation between the two time series is calculated for each year. Therefore, there are 24 correlations (10 for GSWP-2) for each grid point. Before calculating their correlation, the seasonal cycle and linear trend in the two time series is removed to eliminate the influence of a possible long term external forcing, or any influence from the previous period, such as an anomalous wet or dry spring. This calculation method tries to describe

the S-P relation in *this period*. The variation of the soil moisture at top 2 m can be regarded as a red noise process, and the cumulative precipitation is in fact a 30-day running average of the precipitation and is also a red noise process. Their long-term lagged correlation in a whole season in fact removes the weather scale processes and reflects an S-P relation in the whole season. We focus on the boreal summer because most of the Earth's land mass is in the northern hemisphere, so the S-P relation in southern hemisphere midlatitudes is not a true "warm season relationship". This should be kept in mind when examining the results.

This calculation method is based on the assumption that the soil moisture in a certain day will have some influence on the precipitation in subsequent days. However, this method alone cannot determine that the S-P correlation is due to the influence of soil moisture or due to the natural variability of precipitation, because precipitation has direct influence on soil moisture. Findell and Eltahir (1997) tried to isolate these two effects by comparing the S-P correlation with the correlation of past (21-day) precipitation and future precipitation. We will use model experiments to isolates these effects.

3.4.2 Results from reanalyses and GSWP-2

The calculated average S-P correlations for all the years are shown in Figure 3.6. It is a little surprising that the correlations are dominantly negative. Some positive values appear in the dry areas, such as North and South Africa and West Asia. As for the United States, the lowest values appear in the wet Southeast, and the drier West has higher values. In calculating the correlations, we have tried to change the number of subsequent days of cumulative precipitation from 30 to 40 or 20, or change the total precipitation into

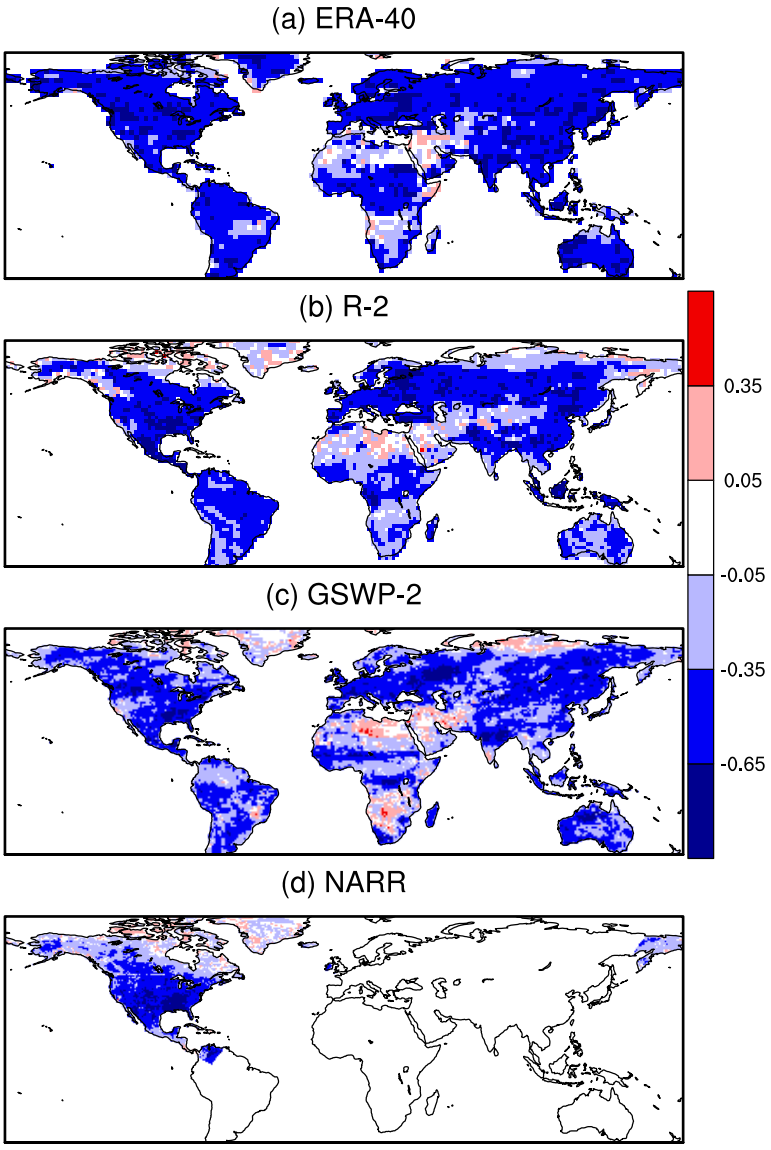

Figure 3.6 The summer average S-P correlation from (a) ERA-40, (b) R-2, (c) GSWP-2, and (d) NARR datasets. All the data is on their native grid. See text for the calculation method. Only the average correlations over the 95% significance level (absolute values larger than 0.05) are shown.

convective precipitation, or the number of days with convective precipitation. No significant pattern change is found, and there are high correlations between these different calculations. Is this dominant negative correlation caused by S-P feedbacks or other reasons? We continue to investigate it with a global climate model.

3.4.3 CAM3 model and experiments

The model used is the NCAR CAM3-CLM3 (Collins et al. 2006) at T42 resolution, a state-of–the-art climate model with sophisticated dynamics and physics. Its land component, CLM3, is a physically based multilayer soil-vegetation-atmosphere transfer model (Oleson et al. 2004). The first simulation (Cnt) is a control run from 1979 to 2002, and is forced by observed interannual varying SSTs. In the second simulation (Cnt_s), the model restarts the control run from June 1 of each year and integrates for 3 month to August 31. The difference is at every time step the soil water in the ET calculation (in fact soil evaporation and vegetation transpiration) is given as its climatological mean values at that time step from the control run, but soil water at other parts of the model is not modified. In this way, the soil moisture still responses to precipitation forcing but the anomalous wet or dry soil moisture does not have any influence on precipitation. Thus the calculated S-P correlation in the second run (Cnt_s) is an S-P relation without soil moisture feedback. By comparing the results from two experiments, we can determine how much S-P correlation is from soil moisture feedback, and how much exists even without feedback.

3.4.4 CAM3 results

The S-P correlations from the two CAM3 experiments and their difference are shown in Figure 3.7. The general patterns of the correlation from the two experiments are very close, and are also close to that in the above analyzed datasets (Figure 3.6). The similarity of the patterns from the two experiments indicates that soil moisture feedback is not the main cause of the dominant negative correlation. Although the two experiments obtain similar correlation patterns, they still have some regional differences (Figure 3.7c). The difference between the two experiments separates the S-P correlation without feedback (Cnt_s) from the total S-P correlation (Cnt) and is the contribution of soil moisture feedback to the S-P correlation, which is in fact the "true" influence of soil moisture feedback on future precipitation. In Figure 3.7c, the positive differences mean soil moisture has a positive influence on future precipitation, and vice versa for the negative differences. Although most of the influence is positive, there is still some regions show negative influence. The negative soil moisture feedback has been found in some observational and modeling studies (Giorgi et al. 1996; Findell and Eltahir 2003; Wu et al. 2006), and some is related to nonlocal feedbacks (Meehl 1994).

The regions with significant differences in Figure 3.7c are the regions that soil moisture feedback may be important for the S-P correlation. These regions are a little different from those regions of strong S-P coupling obtained from GLACE. The reason may be that the calculation method focuses on the impact of current day soil moisture on future 30-day precipitation, which is different from that of GLACE. As the results obtained here is from only one imperfect model, the regional specifics will not be discussed here.

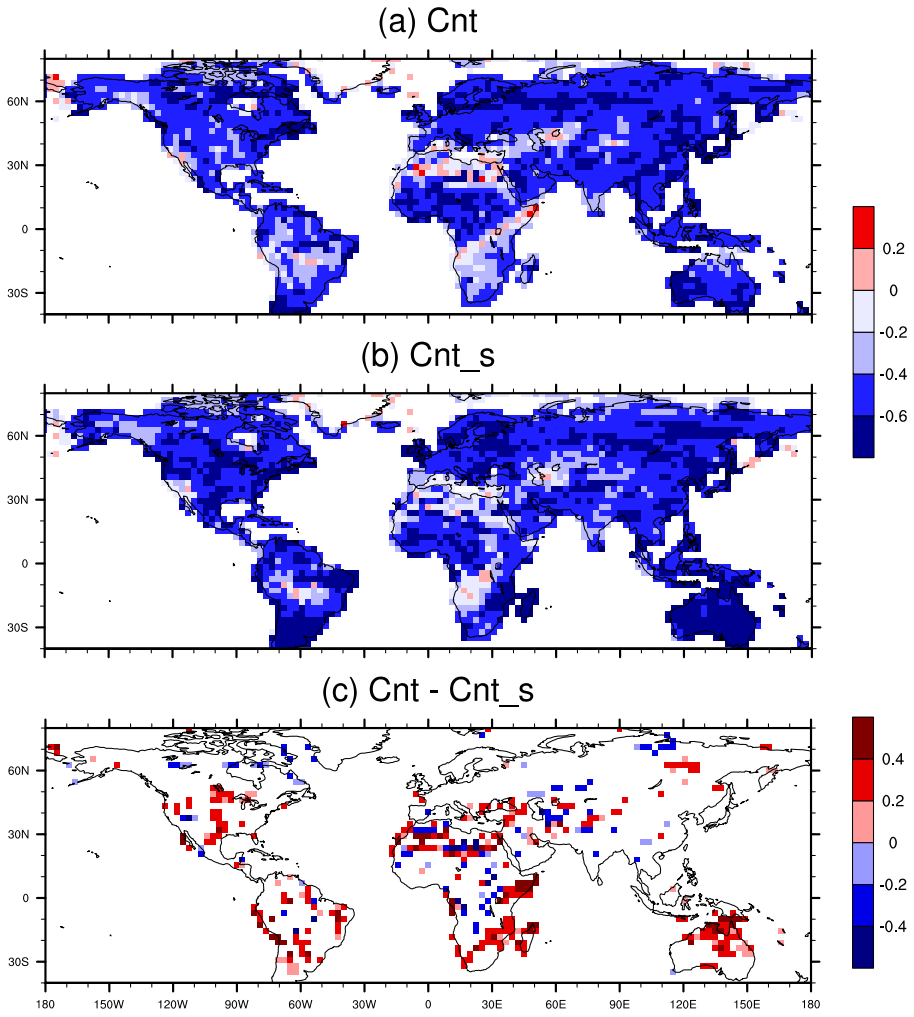

Figure 3.7 The average S-P correlations from the CAM3 simulations (a) Cnt and (b) Cnt_s. Their difference is shown in (c) Cnt – Cnt_s. Only the differences over the 95% significance level are shown in (c).

3.5 Discussion

3.5.1 Autocorrelation of precipitation

From the above experiments we have known that the globally widespread negative S-P correlations are not mainly caused by soil moisture feedback. The GSWP-2 data is produced from land models forced by given precipitation and atmospheric data, and also produces such a negative correlation. Evidently, the land forced by a given precipitation can produce a negative lagged S-P correlation in a summer season, regardless of the regional circulation. What is the cause of this relationship?

Figure 3.8 shows the average correlation between past 21-day (including present day) accumulated precipitation and subsequent 30-day accumulated precipitation. It can be seen that the correlation is mainly negative, with only a few positive correlations in North Africa. Thus there is a tendency for a negative correlation between previous and subsequent precipitation. It is very possible that the negative S-P correlation is related to this. We then calculated the correlation between past 21-day accumulated precipitation and the soil moisture of the current day. It can be seen in Figure 3.9 that their correlation is dominantly positive. We also change the 21-day to 11-day or 5-day in the calculation, and no large change in the correlation pattern is found. It is evident that the information of past precipitation is stored in the current soil moisture, which leads to a negative correlation between soil moisture and subsequent precipitation. Therefore, the negative S-P correlation is caused by the combined effect of the negative autocorrelation of precipitation and the memory of soil moisture. In the dry areas like North Africa and Arabia both of these two effects are weak, so there is no significant S-P correlation. We

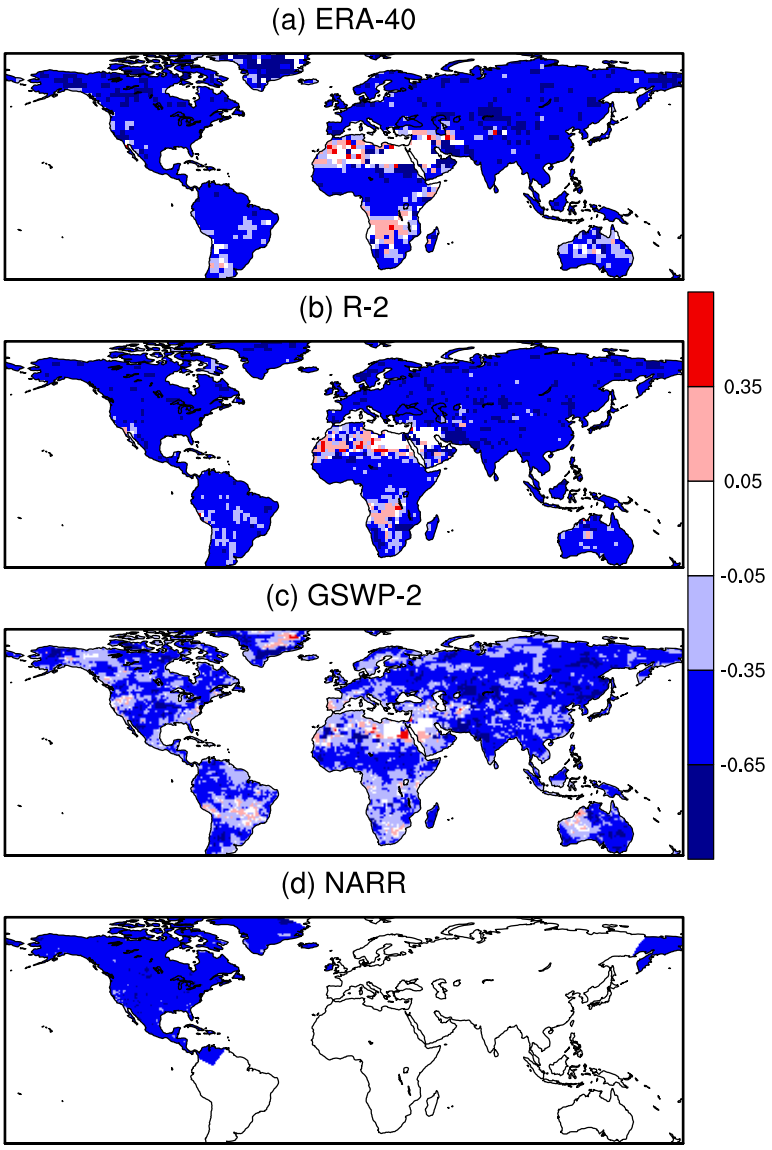

Figure 3.8 Same as Figure 3.6, but for the correlation between past 21-day accumulated precipitation and subsequent 30-day accumulated precipitation.

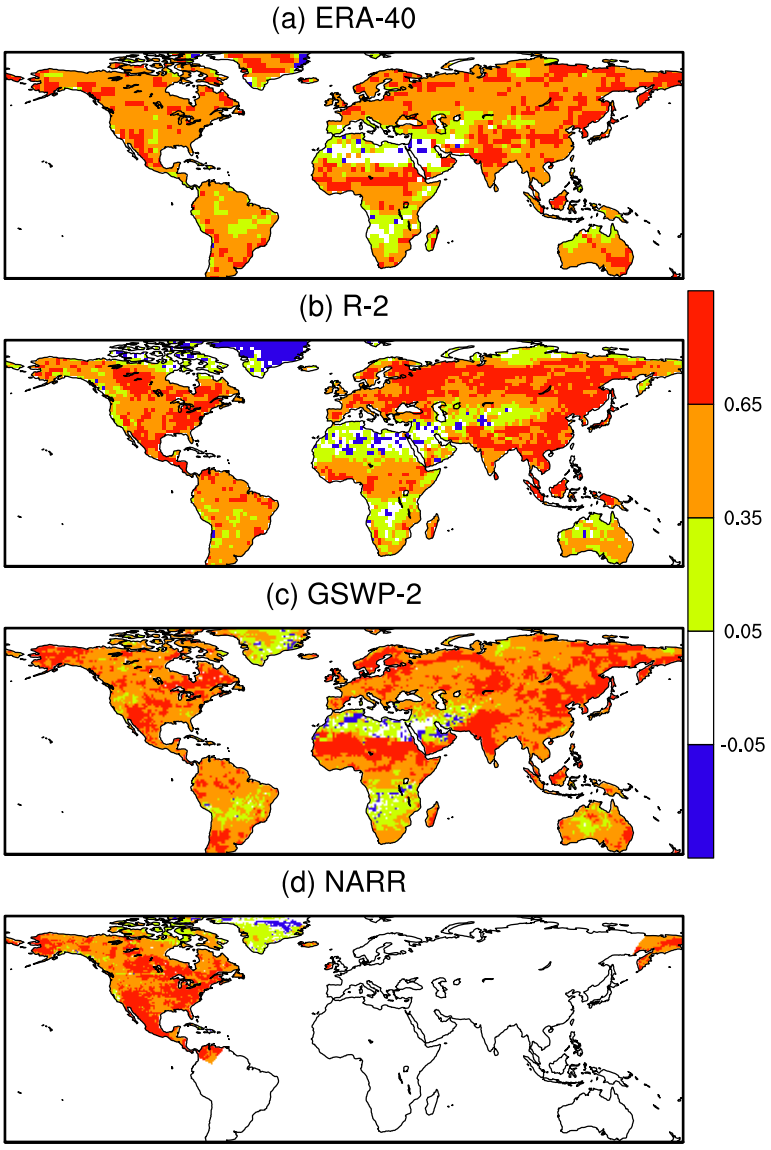

Figure 3.9 Same as Figure 3.6, but for the correlation between past 21-day accumulated precipitation and soil moisture in current day.

also looked at the results from the two CAM3 experiments. They both show similar patterns as that in Figure 3.8 and 3.9 (not shown). This indicates that soil moisture feedback does not play an important role in the two effects, and so the S-P correlation. The above analysis discovered a negative correlation between past 21-day accumulated precipitation and subsequent 30-day accumulated precipitation. What is the cause for this? We will analyze it theoretically.

3.5.2 Theoretical analysis

Although the precipitation time series is close to random and usually contains all kinds of periods, the correlations are determined by the strongest periods. The daily precipitation anomaly *P(t)* in a summer season can be assume to be a sine wave of period *T*:

$$P(t) = \overline{P} \sin \frac{2\pi t}{T}, \tag{3.1}$$

where *t* is time, $\overline{P}$ is the average precipitation anomaly in the season. For each day *t*, the accumulated precipitation anomaly in the subsequent 30 days, $P_{30}(t)$, is calculated as

$$P_{30}(t) = \int_{1}^{30} P(t+\tau) d\tau = \int_{1}^{30} \overline{P} \sin \frac{2\pi(t+\tau)}{T} d\tau . \tag{3.2}$$

The accumulated precipitation anomaly in the past 21 days, $P_{-21}(t)$, can be calculated similarly as

$$P_{-21}(t) = \int_{-20}^{0} \overline{P} \sin \frac{2\pi(t+\tau)}{T} d\tau . \tag{3.3}$$

The soil water anomaly in a certain day, *S(t)*, can be roughly determined by the precipitation anomaly in the past days (Koster and Suarez 1996; Scott et al. 1997):

$$S(t) = a\lambda \int_0^\infty P(t-\tau)e^{-\lambda\tau} d\tau \,, \tag{3.4}$$

where *a* is a scale parameter, $1/\lambda$ is the timescale of surface moisture retention, and is related with soil and vegetation characteristics and local climate. This formulation considers the different weight of past precipitation on the current precipitation, and more recent precipitation has more weight.

The integrations (3.2)-(3.4) can be calculated (see Appendix). It is not difficult to find that $P_{30}(t)$, $P_{-21}(t)$, and *S(t)* all have the same period *T* as *P(t)*, but there are phase shifts. Figure 3.10 shows their respective phase differences with the original precipitation time series *P(t)*. We select λ=0.1 and 2 as two cases of different soil moisture memory, one is very large and one is very small. It can be seen that $P_{30}(t)$ leads *P(t)* while the other three lags the *P(t)*. This is reasonable considering their calculation methods. λ=0.1 has larger phase lag than that of λ=2 because of its longer timescale of soil moisture retention ($1/\lambda$).

As the different time series have the same period, their correlations can be judged from their phase differences. If two time series have the same phase, their correlation will be 1. If their phase difference is π, their correlation will be -1. Figure 3.11 shows the phase difference between $P_{30}(t)$ and *S(t)* (with λ=0.1 and λ=2) and $P_{-21}(t)$. Phase differences larger than π or smaller than 0 are transformed to 0-π for easy comparison. It can be seen that the phase differences have strong fluctuations for periods less than 30 days. As the precipitation time series usually have a wide spectrum, it is useful to look at

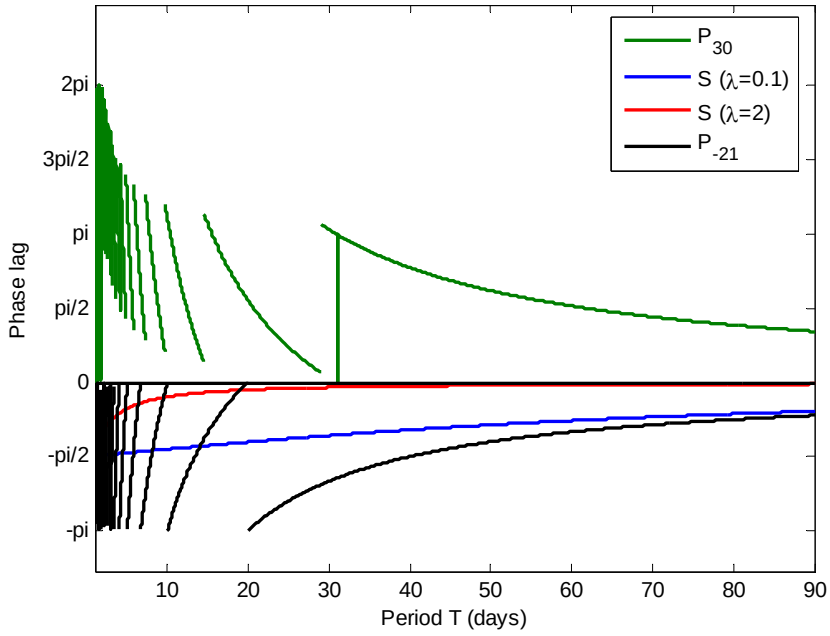

Figure 3.10 The phase difference between the original precipitation time series *P(t)* and future 30-day accumulated precipitation $P_{30}(t)$ (green line), soil water *S(t)* with λ=0.1 (blue line), λ=2 (red line), and past 21-day accumulated precipitation $P_{-21}(t)$ (black line) for different period *T*. Positive values denote leading *P(t)*, and vice versa for the negative values.

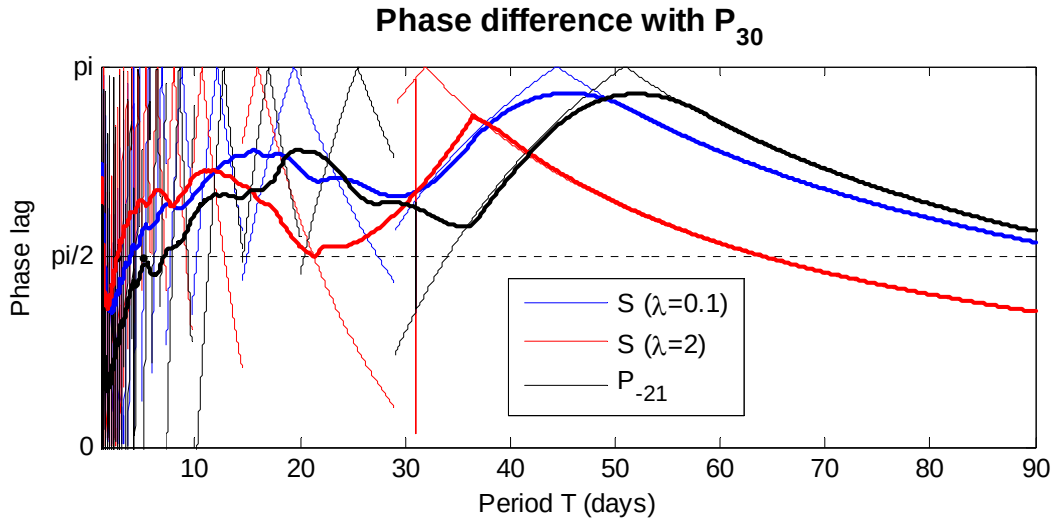

Figure 3.11 The phase difference between future 30-day accumulated precipitation $P_{30}(t)$ and soil water *S(t)* with λ=0.1 (blue line), λ=2 (red line) and past 21-day accumulated precipitation $P_{-21}(t)$ (black line). The thin lines are the calculated values and the thick lines are their respective 15-day running averages. All phase differences are transformed to 0-π.

the running averages of the phase differences. For periods larger than a week, most of the phase differences are between $\pi/2$ and π, which leads to a negative correlation between $P_{30}(t)$ and *S(t)* or $P_{-21}(t)$. This explains the negative-dominant correlations we obtained from the data analysis. Although the phase differences for λ=0.1 and λ=2 interwind, for most of the periods λ=0.1 is closer to π than λ=2. This indicates that at the same precipitation forcing the wet areas or areas with longer soil moisture retention time have more significantly negative correlation.

The above theoretical analysis assumes that the precipitation time series has only one wave, which is usually not true in nature. For multiple waves, the theoretical analysis becomes very difficult. I looked at some examples and found that the waves with larger period and/or amplitude are more important for determining the correlations. Large periods are important because the small periods are easier to be offset when calculating the accumulated precipitation. For a wave of certain period in the multi-wave time series, it also obeys the rule from one-wave analysis.

3.5.3 Test of theory

In the above theoretical analysis, we have found the periods of precipitation oscillation that can cause significantly negative S-P correlation. The next question is whether such periods really exist in the precipitation time series. Two methods are used to analyze the spectrum of precipitation: the power spectrum analysis and autocorrelation. A sample is given in Figure 3.12. It shows the precipitation power spectrum and autocorrelation of a grid point in Russia which has a significantly negative S-P correlation of -0.82 (Figure 3.6c). In Figure 3.12a, its strongest power is at the 30-50 day

period, where the phase difference between $P_{30}(t)$ and *S(t)* is very close to π, especially for λ=0.1 which may be closer to the real condition there. In Figure 3.12b, the average autocorrelation at 15-25 day (half of period) time lag is negative, which indicates an oscillation at 30-50 day period.

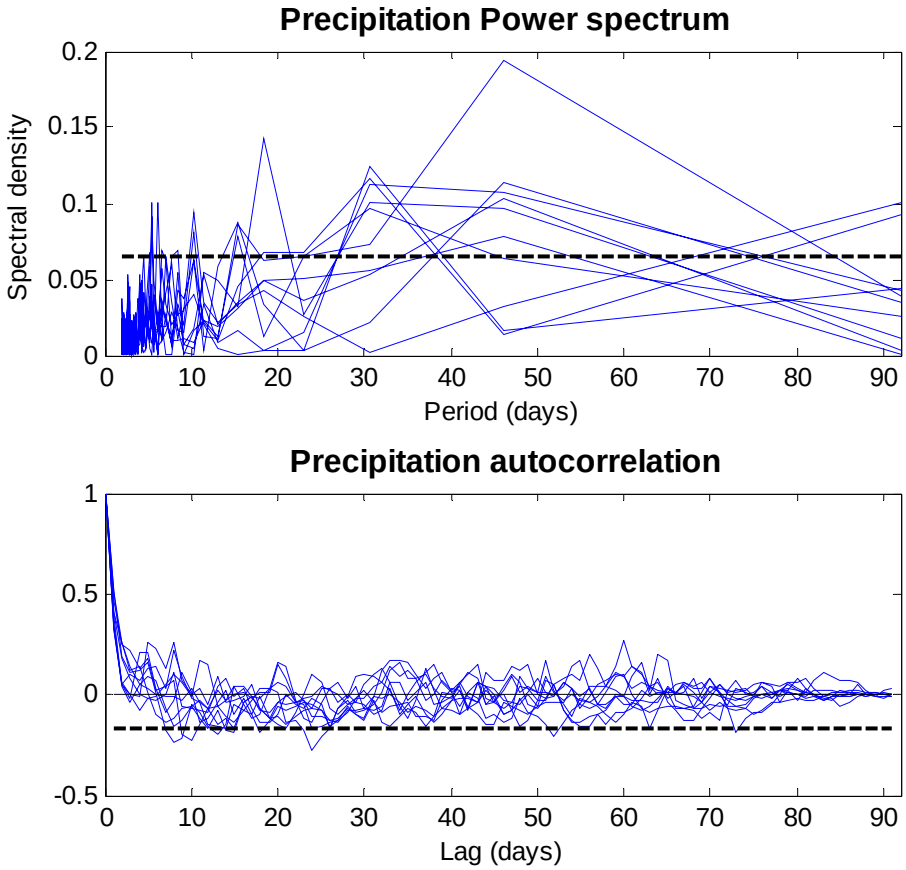

Figure 3.12 The (a) power spectrum and (b) autocorrelation of GSWP-2 JJA daily precipitation for a grid point in Russia (50ºE, 55ºN). The blue lines are for each year of 1986-1995, the dashed lines are their 95% significance level against white noise.

It can be seen in Figure 3.11 that there are some period bands where their phase differences are closer to π than other periods, which indicates more significantly negative S-P correlations. In 32-60 day band, their phase difference is closest to π, and the next is 10-20 day band. As talked about above, the large period is more important for determining the correlations. Thus the 32-60 day period is selected to show the spatial distributions. The spatial distribution of the precipitation spectrum can be compared with the spatial distribution of the S-P correlation to see whether there is some similarity. If there is, our theory is partly supported, although there is possibility that the periods that determines the correlation is in another band, like 10-20 day.

The spatial distribution of the precipitation spectrum is calculated using the two methods talked about above: the power spectrum analysis and autocorrelation. The power spectrum analysis is based on discrete Fourier transform, so the power is shown at discrete periods … 23, 30.67, 46, 92 (Figure 3.12a). The power at the period of 46 days is selected because the surrounding periods are closest to the 32-60 day band. The lag 16-30 day autocorrelation, which reflect the 32-60 day oscillation, is also calculated to show spatially. The GSWP-2 data is used as an example. It can be seen in Figure 3.13 that although the spatial distributions of the power spectrum and autocorrelation are not exactly the same as the spatial distribution of S-P correlation, enough similarity is found among them, such as in Mexico, Indian, Europe, part of Russia and South America. Do not forget that the precipitation variability is only one factor that determines the S-P correlation, and the soil moisture memory may also play a role. The 32-60 day oscillation is also not the only oscillation that influences the S-P correlation; it is only the oscillation that can lead to most significant correlations. Considering these factors, the consistency

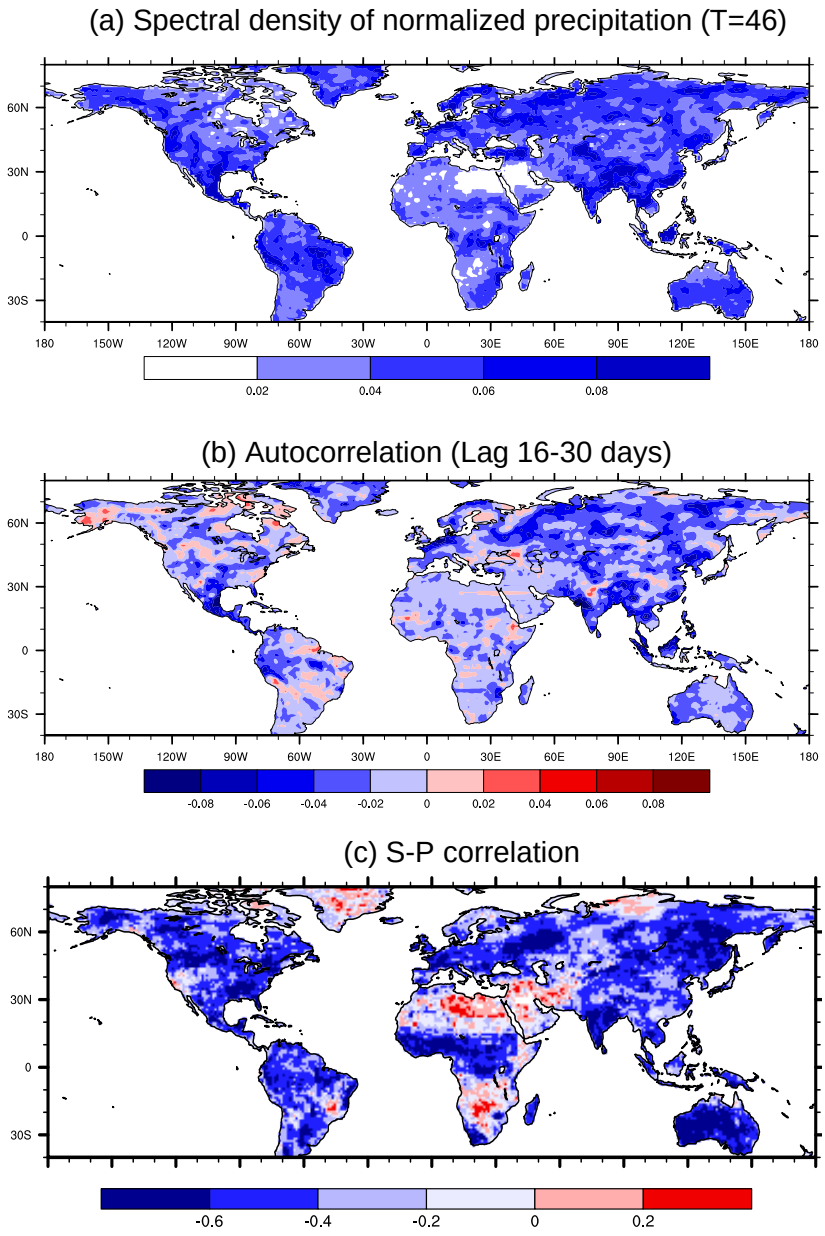

Figure 3.13 (a) Average spectral density of normalized precipitation at the period of 46 days. The 95% significance level against white noise is 0.06. (b) Average precipitation autocorrelation of lag 16-30 days. (c) S-P correlation from Figure 3.6c. All the calculations use the 10 year daily GSWP-2 data in JJA.

found in Figure 3.13 is good enough to support our theory.

In fact, intraseasonal oscillations widely exist in the atmosphere. The Madden-Julian oscillation (MJO; Madden and Julian, 1971, 1972; Madden and Julian, 1994; Zhang, 2005) --- 30-60 day oscillation in the tropics is a famous example. The significant S-P correlation over the tropical land may be caused by it. In addition, the 30-60 day oscillation is also found to exist in the United State (Ye and Cho, 2001), China (Wang et al. 1996a), Europe (Wang et al. 1996b), and even the globe (Donald et al., 2006; Ghil and Mo, 1991; Dickey et al. 1991).

As this correlation pattern in summer is found to be mainly caused by the precipitation oscillation and have nothing to do with soil moisture feedback, this correlation pattern should also exist in other seasons. This conjecture is proved by data analysis (not shown).

We have shown that the spatial distribution of the 32-60 day precipitation oscillation has some similarity to the S-P correlation pattern. Next, we will use a model show that it really contributes to the negative S-P correlation. Two offline experiments are performed with CLM3, the land model of NCAR CAM3. The first is forced by the atmospheric forcing data from Princeton University (Sheffield et al. 2006) and integrated over the period of 1981-2000. The second is the same as the first one except the 32-60 day oscillation in the precipitation forcing is removed. The difference between the two then reflects the impact of the 32-60 day precipitation oscillation. The impact of land feedback is not considered here because it is already shown not to be the determinant factor. The calculated S-P correlation in each experiment and their difference are shown in Figure 3.14. It can be seen that the simulated correlation patterns from the two

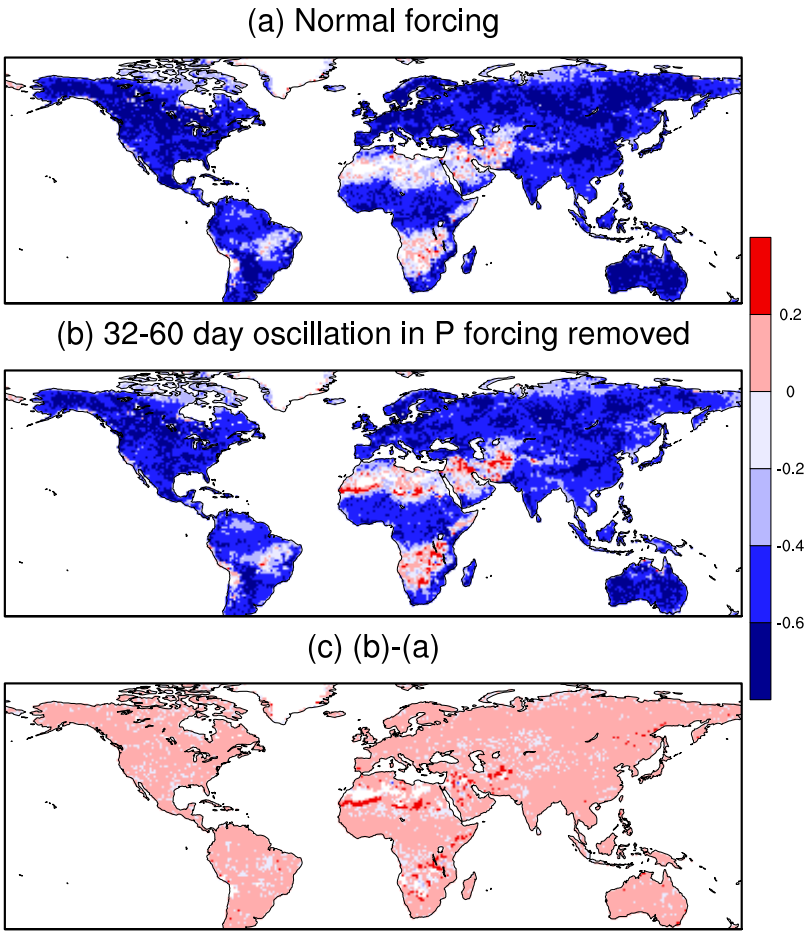

Figure 3.14 The calculated S-P correlations in two offline experiments with CLM3 and their difference. (a) Normal atmospheric forcing from Sheffield et al. 2006. (b) The 32-60 day oscillation in the precipitation forcing is removed. (c) The difference (b)-(a).

experiments are similar to that from other datasets. When the 32-60 day oscillation in precipitation is removed, the global correlations are closer to positive (Figure 3.14c). This indicates that the 32-60 day precipitation oscillation contributes to negative correlation correlations. Then the theory is further supported.

3.5.4 Relation to spatial scale

The S-P correlations are calculated on each grid point, from 0.3° to 2.8°. An interesting question is how the correlations will change on larger spatial scales. We choose a large region on Eurasian continent (35°-65°N, 20°-120°E) and calculate the correlation on different spatial scales. The change of correlation with the spatial scale is shown in Figure 3.15. It can be found that the strongest negative correlation occurs at an intermediate spatial timescale. Obviously, the correlation is influenced by both the temporal and the spatial variability of precipitation. An intermediate spatial scale may cancel out the short timescale oscillations in the precipitation time series and make the intraseasonal oscillations stand out, which leads to stronger S-P correlation. A too large spatial scale may cancel out the intraseasonal oscillations, which leads to weaker S-P correlation.

3.6 Summary and conclusions

This paper compares a lagged S-P correlation of boreal summer in three reanalysis products, GSWP-2 data, and CAM3 simulations. Different datasets and CAM3 come to a similar negative-dominant S-P correlation pattern with wet areas having more

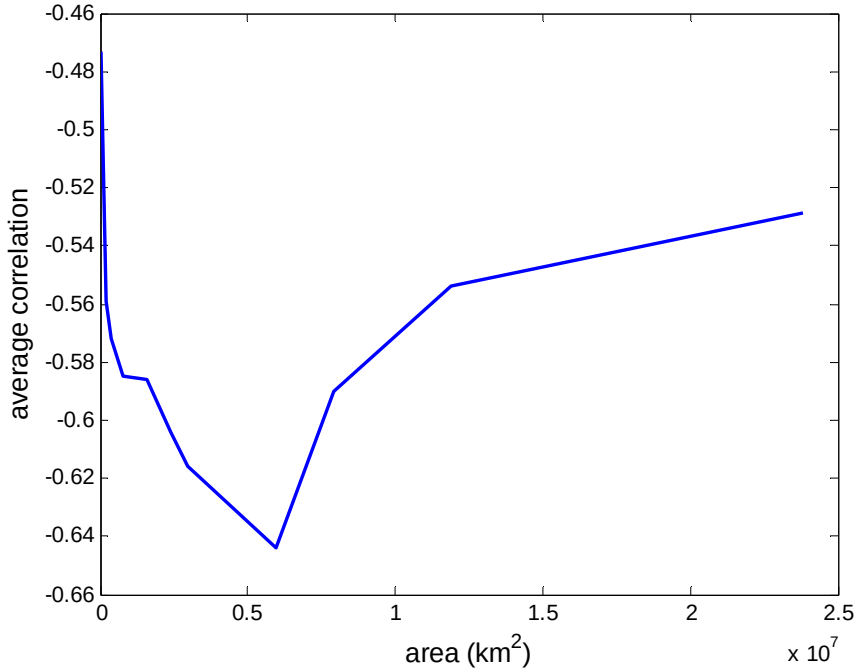

Figure 3.15 The change of S-P correlation with the spatial scale in a large region on Eurasian continent (35°-65°N, 20°-120°E). The correlation is calculated as the average of the subregions in the large region. The horizontal axis shows the area of the subregion.

significantly negative correlations than the dry areas. Experiments with CAM3 show that soil moisture feedback is not the main reason for the correlation pattern. Further analysis shows that the correlation pattern is caused by the combined effect of the variability of precipitation and the memory of soil moisture. The precipitation in most land areas tends to have a negative autocorrelation, which is caused by the intraseasonal oscillation of the atmosphere. Soil memory integrates the influence of past precipitation, which leads to a negative lagged S-P correlation. Finally, a theoretical analysis confirms the above results and finds that S-P correlation is related with both the spectrum of precipitation oscillation and the timescale of soil moisture retention. Precipitation time series with the strongest

oscillation at 32-60 day period is most likely to induce a significantly negative S-P correlation, and regions with longer soil water retention time are more likely to have a significantly negative S-P correlation. Analysis of observational data basically supports the theory.

Identifying a feedback process in the highly interactive climate system is very difficult. Whether a feedback is significant depends on whether it is detectable from the background noise. In this analysis, the lagged S-P correlation does not indicate a causal relation between soil moisture and subsequent precipitation. The effect of soil moisture feedback on calculated precipitation intraseasonal variability is much weaker than that from other sources, and is difficult to be separated by analyzing the observational data. Carefully designed model experiments would be a good choice. The model experiments in this study give an example on how to separate a feedback effect in a highly interactive system.

The calculation method in this study encounters a very low signal-to-noise ratio; other calculation methods may not, but still should be done with care. Figure 3.16 shows the lagged S-P correlation in Illinois calculated with the method of Findell and Eltahir (1997). Instead of calculating the correlation in each year then averaging along the years as we did, they calculate the correlation along all the years. Obviously, this calculation method is also affected by the natural variability of precipitation. It can be seen in Figure 3.16 that there is much difference among the three reanalyses and the CAM3, but most of them shows a positive S-P correlation in the warm season. For the case of CAM3 (Figure 3.16d), the results from the two experiments (described in section 3.4.3) is shown. The difference between the two experiments (Cnt-Cnt_s) shows the influence of soil moisture

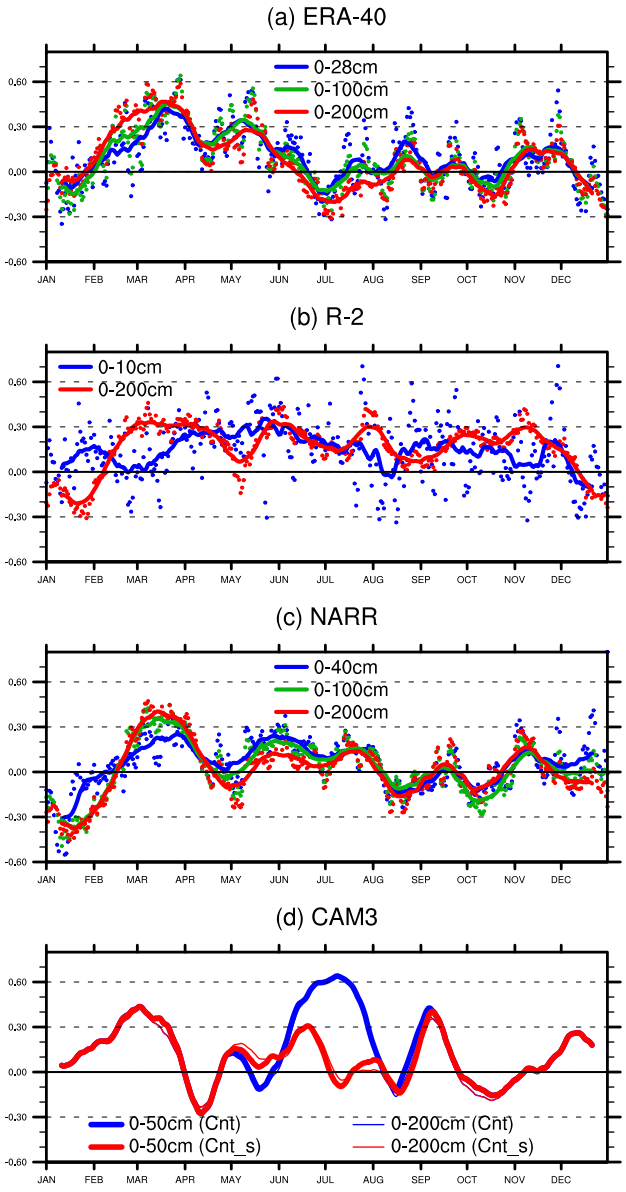

Figure 3.16 The correlation between soil moisture in each day of a year and precipitation in subsequent 30 days in Illinois. The correlation is calculated with the method of Findell and Eltahir (1997). The points are the original correlations, and the lines are 21-day running averages. Correlations with soil water at different depths are shown. The 95% significance level for the original correlation (not the smoothed lines) is 0.404.

feedback on the S-P correlation. It can be seen that soil moisture feedback contributes positively to the S-P correlation. In addition, both of the two experiments show a positive correlation in the warm season. This indicates that even without soil moisture feedback, the S-P correlation is still positive. This will be very intriguing when analyzing the observational data. Therefore, combining data analysis with model simulations would be more reliable to study a causal relation. The study is a warning against misuse of lagged S-P correlation to indicate the influence of soil moisture on precipitation, or similarly using lagged vegetation-precipitation correlation to indicate the influence of vegetation on precipitation. Sometimes a lagged correlation does not indicate a causal relation.

CHAPTER 4

CONCLUDING REMARKS

The main content of the thesis include two parts. The first part developed a one-dimensional model of soil-vegetation-atmosphere interaction to study the dynamics of the land-atmosphere system. The simplicity of the model enables us to perform a series of ideal experiments which may be not possible in global models, such as giving the same external forcing to different land covers, and accurately controlling the forcing. The simplicity of the model also makes it easier to clearly identify the relationships in the complex system. After the relationships are found, the mechanisms for these relationships are discussed and comparisons with observations or other studies, if available, are made, to evaluate their reasonability or correctness. The main contribution of this study is that it examined an aspect that is less addressed in land-atmosphere interaction study --- the influence of different forcing on land-atmosphere interaction. The influence of land on climate variability mainly lies in it memory, which depends on the atmospheric forcing. The main difficulty to study this problem with climate models or observational data is that the forcing is difficult to be estimated. Our study addressed this problem with a simple model. Although the reliability of the findings needs to be evaluated in future studies, it made a first step toward understanding this problem.

The second part of the thesis used datasets from different sources to study the relationship between current soil moisture and future precipitation. Although none of the datasets is from observations, the atmospheric forcings are observation based and the

consistency between the datasets can give us enough confidence. The traditional view is that the soil moisture should have positive influence on future precipitation through evaporation and convection. However, our calculation shows that their correlation is dominantly negative. Model experiments show that this lagged correlation does not reflect a causal relation, and the "real" influence of soil moisture feedback is still mainly positive. The negative correlation is mainly caused by the oscillations in the atmosphere, such as the 30-60 day oscillation, which is also reflected in the precipitation time series. For majority of the land, the influence of soil moisture feedback on the calculated intraseasonal variability of precipitation is much smaller than that from other sources. In some regions, however, there is indeed significant influence. This study illustrates that a lagged correlation does not always indicate a causal relation.

The two parts of the thesis address different questions in land-atmosphere interaction, but there is one thing in common: they both emphasize the influence of different atmospheric forcing on land. This is a little different from the focus of the community, which is to investigate how land anomalies influence the atmosphere. In fact, these two processes constitute the full land-atmosphere interaction processes and influence each other. Understanding of one process will contribute to the understanding of the other.

The complexity of the land-atmosphere system lies in its heterogeneity and strong nonlinearity. Personally, I think the role land processes in the climate variation is still paid less attention than it should be in current climate research. Future research will reveal more important roles of land in climate variation and prediction.

APPENDIX

THEORETICAL ANALYSIS OF THE S-P RELATION

Eqs. (3.2)-(3.4) can be integrated to get

$$P_{30}(t) = \overline{P}\frac{T}{2\pi}[(\cos\frac{2\pi}{T} - \cos\frac{60\pi}{T})\cos\frac{2\pi t}{T} - (\sin\frac{2\pi}{T} - \sin\frac{60\pi}{T})\sin\frac{2\pi t}{T}], \tag{A1}$$

$$P_{-21}(t) = \overline{P}\frac{T}{2\pi}[(\cos\frac{20\pi}{T} - 1)\cos\frac{2\pi t}{T} + \sin\frac{20\pi}{T}\sin\frac{2\pi t}{T}], \tag{A2}$$

$$S(t) = -\frac{a\overline{P}T\lambda}{\lambda^2 T^2 + 4\pi^2}(2\pi\cos\frac{2\pi t}{T} - T\lambda\sin\frac{2\pi t}{T}). \tag{A3}$$

It is easy to find that the above expressions have the same period of T as $P(t)$ in Eq. (3.1). Their phase difference with $P(t)$ can also be calculated. Assume their phase differences are $\phi_{P_{30}}$, $\phi_{P_{-21}}$, and ϕ_S, respectively, then

$$\tan\phi_{P_{30}} = -\frac{\cos\frac{2\pi}{T} - \cos\frac{60\pi}{T}}{\sin\frac{2\pi}{T} - \sin\frac{60\pi}{T}}, \tag{A4}$$

$$\tan\phi_{P_{-21}} = \frac{\cos\frac{20\pi}{T} - 1}{\sin\frac{20\pi}{T}}, \tag{A5}$$

$$\tan\phi_S = -\frac{2\pi}{T\lambda}. \tag{A6}$$

REFERENCES

Betts R. A., P. M. Cox, S. E. Lee, F. I. Woodward (1997), Contrasting physiological structural vegetation feedbacks in climate change simulations. *Nature* 387, 796–799.

Bonan, G. B., S. Levis, L. Kergoat, and K. W. Oleson (2002), Landscapes as patches of plant functional types: An integrating concept for climate and ecosystem models, *Global Biogeochem. Cycles*, 16(2), 1021, doi:10.1029/2000GB001360.

Brovkin, V., S. Levis., M. F. Loutre, M. Crucifix, M. Claussen, A. Ganopolski, C. Kubatzki, V. Petoukhov (2003), Stability analysis of the climate-vegetation system in northern high latitudes. *Climatic Change*, *57*, 119-138.

Brubaker, K. L., D. Entekhabi, and P. S. Eagleson (1993), Estimation of continental precipitation recycling, *J. Clim.*, *6*, 1077-1089.

Campbell, G. S., and J. M. Norman (1998), *An Introduction to Environmental Biophysics*, 2nd ed., 286 pp., Springer-Verlag, New York.

Charney J. G., W. J. Quirk, S-H Chow, J. Kornfield (1977), A comparative study of the effects of albedo change on drought in semi arid regions. *J. Atmos. Sci.*, 34, 1366–1385.

Charney, J.G. (1975), Dynamics of deserts and drought in the Sahel, *Q. J. R. Meteorol. Soc*., *101*, 193–202.

Clapp, R. B. and G. M. Hornberger (1978), Empirical equations for some soil hydraulic properties, *Water Resour. Res.*, *14*, 601-604.

Clark, D. B., Y. Xue, R. J. Harding, P. J. Valdes (2001), Modeling the impact of land surface degradation on the climate of tropical north Africa, *J. Clim.*, *14*, 1809-1822.

Collins, W. D. et al., 2006: The formulation and atmospheric simulation of the Community Atmosphere Model Version 3 (CAM3), *J. Clim.*, 19, 2144–2161.

Cox P. M. and others (1999), The impact of new land surface physics on the GCM simulation of climate and climate sensitivity. *Climate Dynamics*, 15, 183–203.

Cramer, W. et al. (2001), Global response of terrestrial ecosystem structure and function to CO2 and climate change: results from six dynamic global vegetation models. *Global Change Biol., 7***,** 357-373.

D'Odorico, P., F. Laio, and L. Ridolfi (2005), Noise-induced stability in dryland plant ecosystems, *Proc. Natl. Acad. Sci. U. S. A*., *102*, 10819–10822.

Daniel, S. W. (1995), Statistical Methods in the Atmospheric Sciences, 467 pp., Academic Press, San Diego, California, USA.

Deardorff J. W. (1978), Efficient prediction of ground surface temperature and moisture with inclusion of a layer of vegetation. *J. Geophys. Res.*, 83, 1889-1903.

Delire, C., J. A. Foley and S. Thompson (2004), Long-term variability in a coupled atmosphere-biosphere model, *J. Clim.*, *17*, 3947-3959.

Delworth, T. and S. Manabe (1988), The influence of potential evaporation on the variabilities of simulated soil wetness and climate. *J. Clim.*, *1*, 523-547.

Delworth, T. and S. Manabe (1989), The influence of soil wetness on near-surface atmospheric variability. *J. Clim.*, *2*, 1447-1462.

Desborough C. E. (1999), Surface energy balance complexity in GCM land surface models. *Clim. Dyn*., 15, 389-403.

Dickey, J. O., M. Ghil, and S. L. Marcus, (1991), Extratropical aspects of the 40-50 day oscillation in length-of-day and atmosheric angular momentum, *J. Geophys. Res.*, 96, D12, 22,643-22,658.

Dickinson RE, Shaikh M, Bryant R, Graumlich L. 1998. Interactive canopies for a climate model. *J. Clim.*, 11: 2823–2836.

Dickinson, R. E., A. Henderson-Sellers, and P. J. Kennedy (1993), *Biosphere Atmosphere Transfer Scheme (BATS) Version le as Coupled to the NCAR Community Climate Model.* NCAR Technical Note TN383+STR, NCAR, 72 pp.

Dickinson, R. E., A. Henderson-Sellers, P. J. Kennedy, and M. F. Wilson (1986), *Biosphere Atmosphere Transfer Scheme (BATS) for the NCAR Community Climate Model.* NCAR Technical Note TN-275+STR.

Dickinson, R.E., and P. Kennedy, (1992), Impact on regional climate of Amazonian deforestation, *Geophys. Res. Lett.*, *19*, 1947-1950.

Dingman, S. L. (2002), *Physical Hydrology*, 2nd ed., 646 pp., Prentice Hall, New Jersey.

Dirmeyer, P. A. (2003), The role of the land surface background state in climate predictability. *J. Hydrometeor.*, 4, 599-610.

Dirmeyer, P. A., 2000: Using a global soil wetness data set to improve seasonal climate simulation. *J. Climate*, 13, 2900–2922.

Dirmeyer, P. A., and M. Zhao, 2004: Flux replacement as a method to diagnose coupled land–atmosphere model feedback. *J. Hydrometeor*., 5, 1034–1048.

Dirmeyer, P. A., R. D. Koster, and Z. Guo, 2006a: Do global models properly represent the feedback between land and atmosphere? *J. Hydrometeor.*, 7, 1177-1198.

Dirmeyer, P. A., X. Gao, M. Zhao, Z. Guo, T. Oki, and N. Hanasaki, 2006b: GSWP-2: Multimodel Analysis and Implications for Our Perception of the Land Surface, *Bull. Amer. Meteor. Soc*., 87, 1381-1397.

Donald, A., and others, (2006), Near-global impact of the Madden-Julian Oscillation on rainfall, Geophys. Res. Lett., 33, L09704, doi:10.1029/2005GL025155.

Dorman, J. L., and P. J. Sellers, 1989: A global climatology of albedo, roughness length, and stomatal resistance for atmospheric general circulation models as represented by the Simple Biosphere model (SiB). *J. Appl. Meteor.*, 28, 833–855.

Douville, H., 2003: Assessing the influence of soil moisture on seasonal climate variability with AGCMs. *J. Hydrometeor.*, 4, 1044–1066.

Ek, M. B., K. E. Mitchell, Y. Lin, E. Rogers, P. Grunmann, V. Koren, G. Gayno, and J. D. Tarpley, 2003: Implementation of Noah land surface model advances in the

National Centers for Environmental Prediction operational mesoscale Eta model. *J. Geophys. Res.,* 108, 8851, doi:10.1029/2002JD003296.

Eltahir, E. A. B. (1996), The role of vegetation in sustaining large-scale atmospheric circulations in the tropics, *J. Geophys. Res.*, *101*, 4255-4267.

Eltahir, E. A. B. (1998), A soil moisture--rainfall feedback mechanism, 1. Theory and observations, *Water Resour. Res*., *34*, 765-776.

Eltahir, E. A. B. and R. L. Bras (1996), Precipitation recycling, *Rev. Geophys*. *34*, 367-378.

Entekhabi, D., I. Rodriguez-lturbe and R. L. Bras (1992), Variability in large-scale water balance with land surface-atmosphere interaction, *J. Clim.*, 5(8), 798-813.

Fennessy, M. J., and J. Shukla, 1999: Impact of initial soil wetness on seasonal atmospheric prediction. *J. Clim.*, 12, 3167–3180.

Findell, K. L., and E. A. B. Eltahir, 1997: An analysis of the soil moisture-rainfall feedbacks, based on direct observations from Illinois, *Water Resour. Res.*, 33, 725-735.

Findell, K. L., and E. A. B. Eltahir, 2003: Atmospheric controls on soil moisture-boundary layer interactions. Part II: feedbacks within the continental United States. *J. Hydrometeor.*, 4, 570-583.

Foley, J. A., I. C. Prentice, N. Ramankutty, S. Levis, D. Pollard, S. Sitch, A. Haxeltine (1996), An integrated biosphere model of land surface processes, terrestrial carbon balance, and vegetation dynamics, *Global Biogeochem. Cycles*, *10***,** 603-628.

Fu, C. B. (2003), Potential impacts of human-induced land cover change on East Asia monsoon, *Global Planet. Change*, *37*, 219-229.

Gao, X., and P. A. Dirmeyer, 2006: A Multimodel Analysis, Validation, and Transferability Study of Global Soil Wetness Products. *J. Hydrometeor.*, 7, 1218–1236.

Ghil, M., and K. Mo (1991), Intraseasonal oscillations in the global atmosphere. part I: Northern Hemisphere and tropics, *J. Atmos. Sci.*, 48, 752–779.

Gibson, J. K., P. Kållberg, S. Uppala, A. Hernandez, A. Nomura, and E. Serrano, 1997: ERA Description. ECMWF Reanalysis Project Report Series 1, European Centre for Medium-Range Weather Forecasts, Reading, United Kingdom, 77 pp.

Giorgi, F., L.O. Mearns, C. Shields, and L. Mayer, 1996: A Regional Model Study of the Importance of Local versus Remote Controls of the 1988 Drought and the 1993 Flood over the Central United States. *J. Clim.*, 9, 1150-1168.

Grinsted, A., J. Moore, and S. Jevrejeva (2004), Application of the cross wavelet transform and wavelet coherence to geophysical time series, *Nonlinear Proc. Geophys*., *11*, 561-566.

Guo, Z. et al., 2006: GLACE: The global land-atmosphere coupling experiment. Part 2. Analysis, *J. Hydrometeor*., 7, 611-625.

Henderson-Sellers, A., A. J. Pitman, P. K. Love, P. Irannejad, and T. Chen (1995), The Project for intercomparison of land surface parameterisation schemes (PILPS) phases 2 and 3, *Bull. Amer. Meteor. Soc.*, *76*, 489–503.

Hollinger, S. E., and S. A. Isard, 1994: A soil moisture climatology of Illinois. *J. Clim.*, 7, 822-833.

Houghton et al. Eds. Climate Change 2001: The Scientific Basis. Contribution of Working Group 1 to the Third assessment Report of the Intergovernmental Panel on Climate Change, Cambridge University Press, UK. pp 944.

Kalnay E., and M. Cai, (2003), Impact of urbanization and land-use change on climate. *Nature*, 423, 528-531. doi 10.1038/nature01675.

Kalnay, E., and Coauthors, 1996: The NCEP/NCAR 40-Year Reanalysis Project. *Bull. Amer. Meteor. Soc.*, 77, 437–471.

Kanamitsu, M., C.-H. Lu, J. Schemm, and W. Ebisuzaki, 2003: The predictability of soil moisture and near-surface temperature in hindcasts of the NCEP seasonal forecast model. *J. Clim*., 16, 510–521.

Kanamitsu, M., W. Ebisuzaki, J. Woollen, S.-K. Yang, J. J. Hnilo, M. Fiorino, and G. L. Potter, 2002: NCEP– DOE AMIP-II reanalysis (R-2). *Bull. Amer. Meteor. Soc.*, 83, 1631–1648.

Koster, R. D. et al. (2004) Regions of strong coupling between soil moisture and precipitation, *Science*, 305, 1138-1140.

Koster, R. D. et al. (2006), GLACE: The global land-atmosphere coupling experiment, Part 1. Overview, *J. Hydrometeor.* 7, 590-610.

Koster, R. D., and Coauthors (2004), Regions of strong coupling between soil moisture and precipitation, *Science*, 305, 1138-1140.

Koster, R. D., and M. J. Suarez (1995), Relative contributions of land and ocean processes to precipitation variability. *J. Geophys. Res.*, *100*, 13,775-13,790.

Koster, R. D., and M. J. Suarez, 2003: Impact of land surface initialization on seasonal precipitation and temperature prediction. *J. Hydrometeor*., 4, 408–423.

Koster, R. D., M. J. Suarez and M. Heiser (2000) Variance and predictability of precipitation at seasonal-to-interannual timescales, *J. Hydrometeor*., 1, 26-46.

Koster, R. D., M. J. Suarez, R. W. Higgins, and H. M. Van den Dool (2003), Observational evidence that soil moisture variations affect precipitation, Geophys. Res. Lett., 30, 1241, doi: 10.1029/2002GL016571.

Lean, J., and D. A. Warrilow (1989), Simulation of the regional climatic impact of Amazon deforestation, *Nature*, *342*, 411-413.

Levis S., J. A. Foley, D. Pollard (2000), Large scale vegetation feedbacks on a doubled CO2 climate. *J. Clim*.13, 1313–1325.

Levis, S. and G. Bonan (2004), Simulating springtime temperature patterns in the Community Atmosphere Model coupled to the Community Land Model using prognostic leaf area, *J. Clim*., *17*, 4531–4540.

Liu, S. K., S. D. Liu, Z. T. Fu, and S. Lan (2005), A nonlinear coupled soil moisture-vegetation model, *Adv. Atmos. Sci.*, *22*, 337-343.

Liu, Y., and R. Avissar (1999), A study of persistence in the land–atmosphere system with a fourth-order analytical model, *J. Clim*., *12*, 2154–2168.

Liu, Z., M. Notaro, J. Kutzbach, and N. Liu (2006), Assessing global vegetation–climate feedbacks from observation, *J. Clim.*, *19*, 787-814.

Lofgren, B. M. (1995), Sensitivity of land–ocean circulations, precipitation, and soil moisture to perturbed land surface albedo, *J. Clim.*, *8*, 2521–2542.

Lowry, W. P. (1959), The falling rate phase of evaporative soil moisture loss: A critical evalution, *Bull. Am. Meteorol. Soc., 40*, 605.

Madden R. and P. Julian, 1971: Detection of a 40-50 day oscillation in the zonal wind in the tropical Pacific, *J. Atmos. Sci*., 28, 702-708.

Madden R. and P. Julian, 1972: Description of global-scale circulation cells in the tropics with a 40-50 day period. *J. Atmos. Sci.*, 29, 1109-1123.

Madden R. and P. Julian, 1994: Observations of the 40-50 day tropical oscillation: A review. *Mon. Wea. Rev.*, 112-814-837.

Mahrt, L., and H.-L. Pan, 1984: A two layer model of soil hydrology. *Bound.-Layer Meteor.*, 29, 1–20.

Manabe, S. (1969), Climate and the ocean circulation: 1. the atmospheric circulation and the hydrology of the earth's surface, *Mon. Wea. Rew*., 97, 739-805.

McGuire A. D. and others (2001), Carbon balance of the terrestrial biosphere in the twentieth century: analyses of CO2, climate and land use effects with four processes-based ecosystem models. *Global Biogeochemical Cycles*, 15, 183–206.

Meehl, G.A., 1994: Influence of the land surface in the Asian summer monsoon: External conditions versus internal feedbacks. *J. Clim*., 7, 1033--1049.

Mesinger, F. and Coauthors, 2006: North American regional reanalysis, *Bull. Amer. Meteor. Soc*., 87, 343-360.

Mintz, Y. and G. K. Walker (1993), Global fields of soil moisture and land surface evapotranspiration derived from observed precipitation and surface air temperature, *J. Appl. Mete.*, *32*, 1305–1334.

Myneni, R. B., C. D. Keeling, C. J. Tucker, G. Asrar, R. R. Nemani, (1997), Increased plant growth in the northern high latitudes from 1981 to 1991, *Nature*, 386, 698-702.

Oglesby, R. J., S. Marshall, D. J. Erickson, J. O. Roads, and F. R. Robertson (2002), Thresholds in atmosphere-soil moisture interactions: Results from climate model studies, *J. Geophys. Res.*, *107*, D14, 10.1029/2001JD001045.

Oleson, K. W. et al. (2004), Technical description of the Community Land Model (CLM), NCAR Tech. Note NCAR/TN-461+STR, 173 pp., NCAR, Boulder, CO.

Pan, H.-L., 1990: A simple parameterization scheme of evapotranspiration over land for the NMC medium-range forecast model. *Mon. Wea. Rev*., 118, 2500–2512.

Pan, H.-L., and L. Mahrt, 1987: Interaction between soil hydrology and boundary-layer development. *Bound.-Layer Meteor*., 38, 185–202.

Parton W. J., D. S. Schimel, C. V. Cole, D. S. Ojima (1987), Analysis of factors controlling soil organic matter in Great Plains grasslands. *Soil Sci. Soc. Amer. J*., 51, 1173–1179.

Pielke, R.A. Sr., J. Adegoke, A. Beltran-Przekurat, C.A. Hiemstra, J. Lin, U.S. Nair, D. Niyogi, and T.E. Nobis, 2007: An overview of regional land use and land cover impacts on rainfall. *Tellus* B, in press.

Pitman, A. J. (2003), The evolution of, and revolution in, land surface schemes designed for climate models, *Int. J. Climatol.*, *23*, 479-510.

Pollard D., Thompson S. L. (1995), Use of a land-surface-transfer scheme (LSX) in a global climate model: the response to doubling stomatal resistance. *Global Planet. Change,* 10: 129–161.

Robock, A., and Coauthors, 2000: The Global Soil Moisture Data Bank. *Bull. Amer. Meteorol. Soc.*, 81, 1281-1299.

Rodriguez-Iturbe, I, P. D'dorico, A. Porporato and L. Ridolfi (1999a), On the spatial and temporal links between vegetation, climate and soil moisture, *Water Resour. Res.*, *35*, 3709-3722.

Rodriguez-Iturbe, I, P. D'dorico, A. Porporato and L. Ridolfi (1999b), Tree-grass coexistence in savannas: the role of spatial dynamics and climate fluctuations, *Geophys. Res Lett.*, 26, 247-250.

Rodriguez-Iturbe, I., D. Entekhabi, and R. F. Bras (1991), Nonlinear dynamics of soil moisture at climate scales: 1. Stochastic analysis, *Water Resour. Res*., *27*, 1899-1906.

Ruiz-Barradas, A., and S. Nigam, 2005: Warm-season rainfall variability over the US Great Plains in observations, NCEP and ERA-40 reanalyses, and NCAR and NASA atmospheric model simulations. *J. Clim*., 18, 1808-1829.

Ruiz-Barradas, A., and S. Nigam, 2006: Great Plains hydroclimate variability: the view from North American Regional Reanalysis. *J. Clim*., 19, 3004-3010.

Salvucci, G.D., Saleem, J.A., and Kaufmann, R., 2002: Investigating soil moisture precipitation feedbacks with tests of Granger Causality, *Adv. Water Resour*., 25, 1305- 1312.

Scanlon, B. R., D. G. Levitt, R. C. Reedy, K. E. Keese, and M. J. Sully (2005), Ecological controls on water-cycle response to climate variability in deserts, *Proc. Natl. Acad. Sci*., *102*, 6033–6038.

Scheffer, M., S. Carpenter, J. A. Foley, C. Folke, and B. Walker (2001), Catastrophic shifts in ecosystems, *Nature*, *413*, 591-596.

Schlosser, C. A., and D. M. Mocko, 2003: The impact of snow conditions in spring dynamical seasonal predictions. *J. Geophys. Res*., 108, 8616, doi:10.1029/2002JD003113.

Sellers P. J. and others (1996), A revised land-surface parameterization (SiB2) for atmospheric GCMs, Part 1: model formulation. *J. Clim*., 9, 676-705.

Sellers P. J. and others (1997), Modelling the exchanges of energy, water and carbon between continents and the atmosphere. *Science*, 275: 502–509.

Sellers P. J., Y. Mintz, Y. C. Sud, and A. Dalcher (1986), A Simple Biosphere Model (SiB) for use within general circulation models, *J. Atmos. Sci*., 43, 505-531.

Sheffield, J., Goteti, G. and Wood, E.F. (2006), Development of a 50-year high-resolution global dataset of meteorological forcings for land surface modeling. *J. Clim*., 19(13): 3088-3111.

Shukla J., and others (2000), Dynamical seasonal prediction. *Bull. Amer. Meteor. Soc*., 81, 2593-2606.

Taylor, C. M., E. F. Lambin, N. Stephenne, R. J. Harding, R. L. H. Essery (2002), The influence of land use change on climate in the Sahel, *J. Clim.*, *15*, 3615-3629.

Torrence, C., and G. P. Compo (1998), A practical guide to wavelet analysis, *Bull. Am. Meteorol. Soc.*, *79*, 61-78.

Torrence, C., and P. Webster (1999), Interdecadal Changes in the ESNO-Monsoon System, *J.Clim.*, *12*, 2679-2690.

Trenberth, K. E. (1999), Atmospheric moisture recycling: role of advection and local evaporation. *J. Clim., 12*, 1368-1381.

Tsonis, A. A. 1996: Widespread increase in low-frequency variability of precipitation over the past century, *Science*, 382, 700-702.

Uppala, S. M., and Coauthors, 2005: The ERA-40 re-analysis. *Quart. J. R. Meteorol. Soc*., 131, 2961-3012. doi:10.1256/qj.04.176.

Van den Hurk, B. J. J. M., P.Viterbo, A.C.M. Beljaars and A.K. Betts, 2000: Offline validation of the ERA-40 surface scheme. ECMWF Tech. Memo. 295, 42 pp.

Voldoire, A. and J. F. Royer (2004), Tropical deforestation and climate variability, *Clim. Dyn*., *22*, 857-874.

Wang, G. (2004), A conceptual modeling study on biosphere-atmosphere interactions and its implications for physically based climate modeling, *J. Clim.*, *17*, 2572-2583.

Wang, G., and E. A. B. Eltahir (2000a), Ecosystem dynamics and the Sahel drought, *Geophys. Res Lett.*, *27*, 95-98.

Wang, G., and E. A. B. Eltahir (2000b), Modeling the biosphere-atmosphere system: the impact of the sub-grid variability in rainfall interception, *J. Clim*., *13*, 2887-2899.

Wang, G., and E. A. B. Eltahir (2000c), The role of ecosystem dynamics in enhancing the low-frequency variability of the Sahel rainfall. *Water Resour. Res*., *36*, 1013-1021.

Wang, G., E. A. B. Eltahir, J. A. Foley, D. Pollard, and S. Levis (2004), Decadal variability of rainfall in the Sahel: results from the coupled GENESIS-IBIS atmosphere-biosphere model, *Clim. Dyn*., *22*, 625-637, doi: 10.1007/s00382-004-0411-3.

Wang, X. L., C.-R. João., and X., Zhang, (1996a), Intraseasonal oscillations and associated spatial-temporal structure of precipitation over China, *J. Geophys. Res*., 101, D14, 19,035-19,042.

Wang, X. L., C.-R. João., and X., Zhang, (1996b), Low-frequency oscillations and associated wave motions over Eurasia, *Tellus,* A, 48, issue 2, 238-253.

Wei, J., R. E. Dickinson, and N. Zeng, 2006: Climate variability in a simple model of warm climate land-atmosphere interaction, *J. Geophys. Res*., 111, G03009, doi:10.1029/2005JG000096.

Wu, W.R., R.E. Dickinson, H. Wang, Y. Liu, and M. Shaikh, 2006: Covariabilities of spring soil moisture and summertime United States precipitation in a climate simulation, *Int. J. Climatol*., doi:10.1002/joc.1419.

Xue, Y. (1996), The Impact of desertification in the Mongolian and the Inner Mongolian grassland on the regional climate, *J. Clim.*, *9*, 2173-2189.

Xue, Y., and J. Shukla (1993), The influence of land surface properties on Sahel climate. Part I: Desertification, *J. Clim.*, *6*, 2232-2245.

Xue, Y., H.-M. H. Juang, W. Li, S. Prince, R. DeFries, Y. Jiao, R. Vasic (2004), Role of land surface processes in monsoon development: Part I - East Asia and West Africa, *J. Geophy. Res*., *109*, D03105, doi: 10.1029/2003JD003556.

Yang, F., A. Kumar, W. Wang, H.-M. H. Juang, and M. Kanamitsu, 2001: Snow–albedo feedback and seasonal climate variability over North America. *J. Clim*., 14, 4245–4248.

Ye, H. and H.-R. Cho, 2001: Spatial and temporal characteristics of intraseasonal oscillations of precipitation over the United States, *Theor. Appl. Climatol*., 68, 51-66.

Zeng, N. (1998), Understanding climate sensitivity to tropical deforestation in a mechanistic model, *J. Clim*., *11*, 1969-1975.

Zeng, N., and J. D. Neelin (1999), A land-atmosphere interaction theory for the tropical deforestation problem, *J. Clim*., *12*, 857-872.

Zeng, N., and J. D. Neelin (2000), The role of vegetation-climate interaction and interannual variability in shaping the African Savanna, *J. Clim.*, *13*, 2665-2670.

Zeng, N., J. D. Neelin, K.-M. Lau, and C. J. Tucker (1999), Enhancement of interdecadal climate variability in the Sahel by vegetation interaction, *Science*, 286, 1537-1540.

Zeng, X., S. S. P. Shen, X. Zeng, R. E. Dickinson (2004), Multiple equilibrium states and the abrupt transitions in a dynamical system of soil water interacting with vegetation, *Geophys. Res. Lett*., *31*, doi:10.1029/2003GL018910.

Zhang, C. 2005: Madden-Julian Oscillation. *Rev. Geophys.*, 43, 1-36.

Zhang, X., M. A. Friedl, C. B. Schaaf, A. H. Strahler, and Z. Liu (2005), Monitoring the response of vegetation phenology to precipitation in Africa by coupling MODIS and TRMM instruments, *J. Geophys. Res*., *110*, D12103, doi:10.1029/2004JD005263.

Zhao, M., and P. Dirmeyer, 2003: Production and analysis of GSWP-2 near-surface meteorology data sets. COLA Tech. Rep. 159, 22pp. [Available online at ftp://grads.iges.org/pub/ctr/ctr_159.pdf.]

Zheng, X. and E. A. B. Eltahir (1997), The response to deforestation and desertification in a model of West African monsoon, *Geophys. Res. Lett*., *24*, 155-158.

Zhou, L., Tucker, C.J., Kaufmann, R.K., Slayback, D., Shabanov, N.V, and Myneni, R.B., Variations in northern vegetation activity inferred from satellite data of vegetation index during 1981 to 1999, *J. Geophys. Res.*, (2001), 106, 20,069-20,083.

VITA

Jiangfeng Wei

JIANGFENG WEI was born in Hubei, China. He received a B.S. in Meteorology from Nanjing Institute of Technology, Nanjing, China in 1999 and a M.S. in Atmospheric Sciences from Institute of Atmospheric Physics, Chinese Academy Sciences in 2002 before coming to Georgia Tech to pursue a doctorate in Atmospheric Sciences.